

# Generation and detection of plane coherent shear picosecond acoustic pulses by lasers: Experiment and theory

T. Pezeril,<sup>1,\*</sup> P. Ruello,<sup>1</sup> S. Gougeon,<sup>1</sup> N. Chigarev,<sup>1</sup> D. Mounier,<sup>1</sup> J.-M. Breteau,<sup>1</sup> P. Picart,<sup>2</sup> and V. Gusev<sup>1</sup>

<sup>1</sup>Laboratoire de Physique de l'État Condensé, UMR CNRS 6087, Université du Maine, 72085 Le Mans, France

<sup>2</sup>Laboratoire d'Acoustique, UMR CNRS 6613, Université du Maine, 72085 Le Mans, France

(Received 25 January 2007; revised manuscript received 11 April 2007; published 29 May 2007)

Hypersound generation and detection by laser pulses incident on the interface of an opaque anisotropic crystal are theoretically and experimentally investigated in the case where the symmetry is broken by a tilt of its axis of symmetry relative to the interface normal. A nonlocal volumetric mechanism of plane shear sound excitation is revealed and a modification of the temporal shape of the reflectivity signal with variation in probe light polarization is observed, both attributed to asynchronous propagation of the acoustic eigenmodes. Experiments and theory demonstrate the possibility of using polycrystalline materials with an arbitrary distribution of grain orientations for the generation and the detection of picosecond shear ultrasound.

DOI: 10.1103/PhysRevB.75.174307

PACS number(s): 78.20.Hp, 43.35.+d, 68.60.Bs, 78.47.+p

## I. INTRODUCTION

The general tendency in the development of laser ultrasonics, a research field where lasers are used for the excitation of ultrasonic waves,<sup>1,2</sup> is the continuous effort to generate coherent acoustic waves of higher and higher frequencies. Following the advent of ultrafast lasers, picosecond longitudinal-acoustic pulses were generated and detected for the first time in 1984,<sup>3</sup> announcing the emergence of picosecond laser ultrasonics.<sup>4</sup> This technique has found widespread use for studies of ultrafast phenomena and non-destructive testing of submicron thin films and nanostructured materials. Another clear tendency in the development of laser ultrasonics, also stimulated by the demand of non-destructive testing, is the continuous search for methods that excite different types of acoustic waves (e.g., Rayleigh acoustic waves for surface diagnostics<sup>5,6</sup>) or different acoustic wave polarizations (e.g., bulk shear waves for the evaluation of the shear viscosity of fluids or the rigidity of solids<sup>7</sup>).

There is an important difference in the processes of laser generation of longitudinal and shear bulk acoustic waves in isotropic materials when the photoelastic generation is based on the thermoelastic effect (that is, when acoustic waves are excited due to thermal expansion following the absorption of laser radiation). In fact, shear acoustic waves are not excited in an individual heated point of the material volume at all. From the physical point of view, this is the consequence of the isotropy of thermal expansion which proceeds equivalently along all possible directions from the heated point. As a result, the particle displacement preserves spherical symmetry, but a shear deformation is not generated because transverse displacement is orthogonal to this spherically symmetric excitation. Mathematically, this physical observation is expressed in the fact that the thermoelastic stress tensor  $\sigma_{ij} = -K\beta T\delta_{ij}$  is spherical. Here,  $K$  is the bulk elastic modulus,  $T$  is the temperature rise,  $\beta$  is the volumetric thermal-expansion coefficient, and  $\delta_{ij}$  denotes the Kronecker delta (or unit tensor). The density of thermoelastic forces acting in the inhomogeneously heated isotropic material can be written in the form  $\vec{f} = -K\beta\vec{\nabla}T$ . Consequently, the ther-

moelastic forces in isotropic media are potential forces and, as a result, they excite only the potential part of the particle velocity field associated with longitudinal-acoustic waves. If the velocity of the particle is represented in the form  $\partial\vec{u}/\partial t = \vec{\nabla}\phi + \vec{\nabla}\times\vec{\psi}$ , where  $\vec{u}$  is the particle displacement vector and  $\phi$  and  $\vec{\psi}$  are scalar and vector potentials, respectively, then, the equation of material motion splits into two parts (see, e.g., Chap. 3 of Ref. 8),

$$\frac{\partial^2\phi}{\partial t^2} - c_L^2\Delta\phi = -\beta^*c_L^2\frac{\partial T}{\partial t}, \quad (1)$$

$$\frac{\partial^2\vec{\psi}}{\partial t^2} - c_S^2\Delta\vec{\psi} = 0, \quad (2)$$

where  $c_L$  and  $c_S$  are the velocities of the longitudinal and shear waves, respectively,  $\Delta$  denotes the Laplace operator, and  $\beta^* = \beta K/\rho c_L^2 = \beta(1 - 4c_S^2/3c_L^2)$  is the effective thermal-expansion coefficient. Equations (1) and (2) explicitly demonstrate that shear acoustic waves are not excited in the volume of a homogeneous isotropic material. However, the scalar and vector potentials (the longitudinal and shear waves) are coupled at the boundaries of the medium.<sup>8</sup> Consequently, shear waves can be excited via mode conversion of the longitudinal waves obliquely incident on the material surface (see Fig. 1).

The difference between longitudinal and shear waves, from the point of view of their thermoelastic generation in the isotropic media described above, leads to additional complexity in the generation of plane shear acoustic waves by lasers. A well-known approach for the generation of plane longitudinal-acoustic waves is to homogeneously illuminate the plane surface of the material at a spatial scale exceeding the characteristic wavelength of the generated ultrasound. In other words, the size of the laser spot focused on the surface of the material should be significantly larger than both the optical heating depth and the distance of acoustic wave propagation during the time of pulsed laser action. In this case, the elementary sources of longitudinal waves are laterally homogeneously distributed in a plane layer beneath the

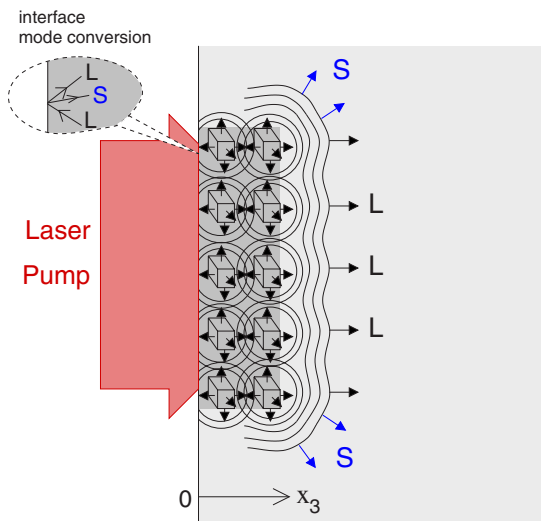


FIG. 1. (Color online) Schematic representation of the near field of thermoelastic acoustic wave generation in an isotropic homogeneous medium. Each point of the heated region is a source of longitudinal waves only. By virtue of symmetry, longitudinal waves from different point sources propagating off the surface normal axis are mutually compensated and no shear waves are excited in normal reflection. Shear waves are excited only near the edges by obliquely incident longitudinal waves.

surface. The particles far from the edges of the laser irradiated region will move predominantly in the direction normal to the surface (see Fig. 1), because all the directions of motion along the surface are locally equivalent. Most of the light absorbing volume operates as a piston expanding normally to the surface (Fig. 1). As a consequence, two plane longitudinal-acoustic waves are excited (one propagating from the surface and another incident on the surface). Unfortunately, the plane longitudinal-acoustic waves normally incident to the surface cannot lead to plane shear acoustic waves via mode conversion. By virtue of symmetry, plane reflected shear waves cannot chose a unique polarization among all equivalent polarizations along the surface, and as a result they are not excited at all. However, shear waves will be excited through mode conversion in the vicinity of the edges of the excited area where longitudinal waves are obliquely incident (see Fig. 1). However, even in the near field, the emitted shear waves are not planar; the predominant emission direction is inclined relative to the surface normal and in general the duration of the nonplanar shear acoustic pulses excited depends on the radius of the laser focus, in addition to the dependence on the laser pulse duration and on the depth of the heated region.<sup>9-11</sup>

Different solutions were proposed to overcome the aforementioned problem of the generation of plane shear waves. One solution, successful in the megahertz frequency regime with the application of nanosecond lasers,<sup>12,13</sup> requires the use of prisms (see Fig. 2). Plane longitudinal-acoustic (LA) pulses are generated in the face of one of the coated prism's faces. This launches LA pulses obliquely incident on the hypotenuse free surface of the prism where plane shear acoustic (TA) pulses are excited via mode conversion by reflection of

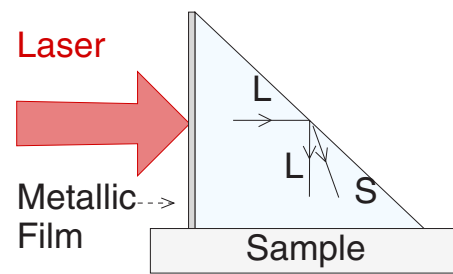


FIG. 2. (Color online) Schematic of the megahertz prism photoelastic transducer. The shear acoustic waves arise from the oblique reflection of the longitudinal waves at the hypotenuse free surface of the prism.

LA pulses.<sup>14</sup> However, scaling to the gigahertz frequency regime of picosecond laser ultrasonics requires a technique of microprism machining and their deposition on the surface of structures that remains to be developed. Because the hypersonic hardly propagates deeper than a few microns at room temperature, the prisms would need to be on the order of  $1 \mu\text{m}$  in size.

Other solutions proposed for the generation of plane shear hypersonic do not require this complicated microgeometry. Electrostriction<sup>7,15</sup> and the inverse piezoelectric effect<sup>16,17</sup> have been proposed for the generation of plane shear acoustic waves in the gigahertz frequency regime. The former can be realized even in an isotropic medium,<sup>7</sup> while the latter requires laser irradiation of single crystals, but does not require disorientation of the material crystallographic axis relative to the surface normal. It is always necessary to break the symmetry of the system in order to generate shear waves. In the cases of electrostriction and piezoelectric effects, the symmetry is broken at the level of the forces inducing the material motion.

Returning to the thermoelastic excitation of acoustic waves, it has been proposed to break the symmetry of the system by using interface mode conversion between the isotropic material where plane LA waves are generated and an anisotropic material with the crystallographic axis disoriented relative to the interface normal. In this case, plane transverse waves are excited in reflection<sup>18</sup> and plane quasi-transverse waves are excited in transmission<sup>19</sup> through the interface mode conversion of plane LA pulses, even those which are normally incident.

Finally, it has been proposed to break the symmetry at the level of the thermoelastic force by using materials with anisotropic thermal-expansion coefficients  $\beta_{ij}^T$ .<sup>20</sup> In the first experiments of this type,<sup>20</sup> the use of hexagonal crystals has been primarily motivated by the static strain relation of the unrestricted expansion of the crystal,  $S_{ij}^T = \beta_{ij}^T T$ , where  $S_{ij}^T$  is the static strain tensor; static shear strain exists only in materials capable of anisotropic thermal expansion, that is, those with nonspherical tensor  $\beta_{ij}^T$ , the lowest symmetry being hexagonal. It should be noted, however, that although shear waves are excited in the case of nonspherical  $\beta_{ij}$  in each point of the laser heated region, nevertheless, in order to achieve emission of plane shear waves normally to the laser irradiated surface it is necessary to break the symmetry at the

level of the surface orientation. The normal to the surface should not coincide with the symmetry axis of the anisotropic material. We label this situation the plane geometry with broken symmetry.

In this paper, the detailed results of experimental and theoretical analyses of laser induced thermoelastic generation and photoelastic detection of hypersound in anisotropic materials are presented in order to describe a general picture of picosecond laser ultrasonics in crystals. A brief report of the obtained results has been published earlier.<sup>21</sup> We show that anisotropic thermal expansion is not necessary for the generation of plane shear waves. Moreover, it is possible to excite plane shear waves in the plane geometry with broken symmetry even in the hypothetical case where the thermoelastic stress tensor in the anisotropic material  $\sigma_{ij} = C_{ijkl}\beta_{kl}^T T$  is spherical. We reveal the mechanism of shear wave excitation by the spherical part  $(\sigma_{kk}/3)\delta_{ij}$  of the non-spherical  $\sigma_{ij}$ , which does not require anisotropic thermal expansion and is operative even in crystals with isotropic thermal expansion, such as cubic crystals. In the general case, the spherical part of the thermoelastic stress can give a more important contribution to plane shear wave excitation than its deviatoric part  $\bar{\sigma}_{ij} = \sigma_{ij} - (\sigma_{kk}/3)\delta_{ij}$ .

Both the theory of thermoelastic generation and of the photoelastic detection in crystals described in this paper, which have been successful in explaining all our experimental observations, carefully take into account two essential features of laser ultrasonics in crystals.

First, in a general case, all three acoustic eigenmodes (one quasilongitudinal and two quasishear) are excited simultaneously through the photoelastic mechanism. Qualitatively speaking, for the physics of the thermoelastic generation it is important that all thermoelastic eigenmodes in the crystals are quasi and that all of them include a longitudinal part. As a consequence, all the eigenmodes can be excited even by isotropic (spherical) stress through the excitation of their longitudinal components. The other important point concerns the asynchrony between the acoustic eigenmodes, in the sense that all three modes are propagating with different velocities. Later on, after the longitudinal strain components are instantaneously launched by the action of the laser, the wave field will be spatially and temporally decomposed into individual acoustic modes revealing shear components.

Second, the asynchrony between the acoustic modes plays an important role in the understanding of the acousto-optic detection process as well. The developed theory relates both the observation of shear pulse anomalous broadening and the observation of the strong dependence of the detected longitudinal pulse profiles on the polarization of the probe laser pulse to the asynchrony in the propagation of acoustic eigenmodes. The theory provides physical insight into why, in our experiments, it was possible to monitor (to generate and to detect) shear hypersound using not only single crystals but also polycrystalline materials with significant variations in individual grain orientations relative to the material surface. The latter observations could be suited for the future applications of picosecond ultrasonics involving shear waves.

The paper is arranged as follows. We present our experimental results in Sec. II. Section III describes a theory of thermoelastic excitation of acoustic waves in a system com-

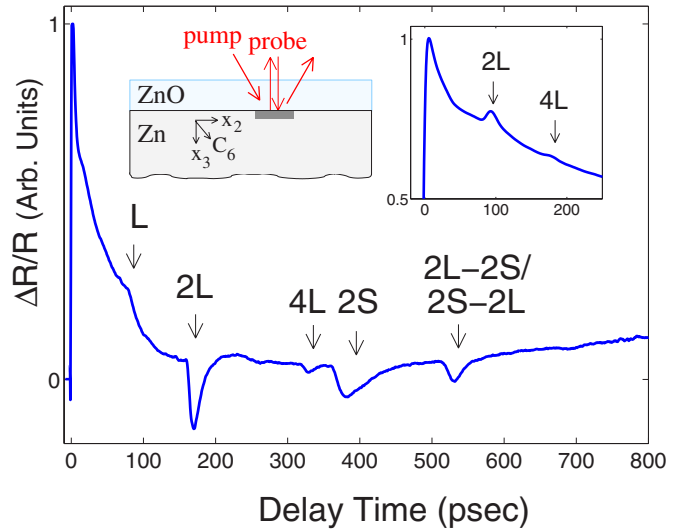


FIG. 3. (Color online) Change in transient reflectivity for a Zn single-crystal substrate with  $C_6$  axis oriented at angle  $\theta \sim 25^\circ$  relative to the interface normal and on which a transparent ZnO film of 270 nm thickness has been deposited. The probe polarization coincides with the  $x_2$  direction. The variation in transient reflectivity presented in the inset corresponds to the case of a Zn single crystal whose normal surface coincides with the  $C_6$  axis.

posed of an isotropic transparent film deposited on an anisotropic opaque material with crystallographic axes disoriented relative to the interface normal (plane geometry with broken symmetry). Section IV is devoted to the theoretical analysis of the photoelastic detection of the acoustic pulses propagating in an anisotropic substrate. We finish by discussion in Sec. V and conclusions in Sec. VI.

## II. EXPERIMENTAL RESULTS

For the picosecond transient reflectivity measurements, we used a common pump-probe configuration (see the inset of Fig. 3) based on a mode-locked femtosecond Ti:sapphire laser operating in the near infrared (800 nm), producing 100 femtosecond pulses at a repetition rate of 76 MHz. The laser beam from the cavity is split into a pump beam and a probe beam, both focused onto an area of the sample  $\sim 40 \mu\text{m}$  in diameter. Each pump pulse of 2 nJ induces a thermal stress in the metallic zinc substrate that gives rise to coherent acoustic waves propagating normally to the ZnO/Zn interface. The time-delayed probe beam (with ten times less energy) is sensitive to the strain induced small variations of the sample reflectivity. The record of the change in reflectivity of the delayed probe beam provides the time resolved acoustic dynamics in the hundreds of picoseconds time scale. Several anisotropic Zn single crystals with the  $C_6$  axis tilted by angles  $\theta$  ranging from  $0^\circ$  up to  $40^\circ$  relative to the surface normal were prepared. The surface was then mechanically polished, leading to a roughness better than 5 nm checked by atomic force microscopy over a surface exceeding  $100 \mu\text{m}^2$ . Each zinc substrate was then coated with a rf sputtered transparent polycrystalline ZnO layer. The important improvement in the structures prepared here compared

with those of Matsuda *et al.*<sup>20</sup> is that transparent ZnO films used here, due to their extremely low photoelastic constants at the optical probe wavelength of 800 nm, do not add a Brillouin component to the observed reflectivity signals (see Fig. 3). Thus, in ZnO/Zn structures, both the excitation and detection of sound take place in the optical penetration depth of the Zn substrate.

Theoretical estimates of the arrival time of the echoes in Fig. 3 permit identification of the various detected acoustic strain pulses from the known thickness and sound velocities (i.e.,  $v_L=6096$  m s<sup>-1</sup> and  $v_S=2736$  m s<sup>-1</sup>) of the ZnO films. The signals denoted by 2L and 4L correspond to the arrival of the longitudinal pulses at the ZnO/Zn interface after crossing the film twice and four times, respectively. The notation 2S is given to shear pulses on their first arrival at the ZnO/Zn interface. The notations 2S-2L/2L-2S are given to pulses arriving after one more round-trip in the film, that is, to the L (S) pulses mode converted in the first reflection at the interface from the 2S (2L) pulses. Additional confidence in the identification of the shear wave arrivals is given by comparison with the signal in the inset of Fig. 3 which was detected in the symmetrical system ( $\theta=0^\circ$ ) where S waves are seen to be absent. These experiments confirm the possibility of direct thermoelastic excitation of S waves as well as their excitation through mode conversion of the echoes (see 2L-2S/2S-2L echoes). Furthermore, an interesting feature of the signal is the different duration of the leading fronts when we compare the longitudinal and shear wave signals. While the first one is rather abrupt, the second one rises and reaches a maximum in about 10 ps. The theory of thermoelastic generation in anisotropic opaque materials presented in the next section will go deeper into the interpretation of the different durations of the leading fronts of the pulses of different polarizations, which cannot be attributed to the difference in longitudinal and shear velocities and to the difference in the absorption of L and S waves only. In particular, the theory reveals a new mechanism of shear wave thermoelastic generation specific to anisotropic media.<sup>21</sup>

Finally, the fact that the probe photoelastic scattering occurs in the anisotropic zinc single crystal gives a remarkable feature of the recorded transient reflectivity signal's dependence on the orientation of the probe's polarization. Figure 4 shows the modifications of the transient reflectivity signal changes accompanying rotation of the probe polarization. Drastic modification of the profile of the 2L echo and of the magnitude of the 2S echo is due to the fact that the detection process takes place in the anisotropic medium where in general all three of the acoustic modes influence light scattering. The theory of photoelastic scattering in anisotropic materials is detailed in Sec. IV. The coincidence of the signals for  $\phi=0^\circ$  and  $180^\circ$ , see Fig. 4, which is equivalent to  $180^\circ$  crystal rotation ( $\theta \rightarrow -\theta$ ), indicates that the symmetry of the detected scattered electric field is higher than the symmetry of the sample geometry. This will be explained when anisotropy is taken into consideration both in the theoretical description of the thermoelastic generation and in the photoelastic detection detailed in the next sections.

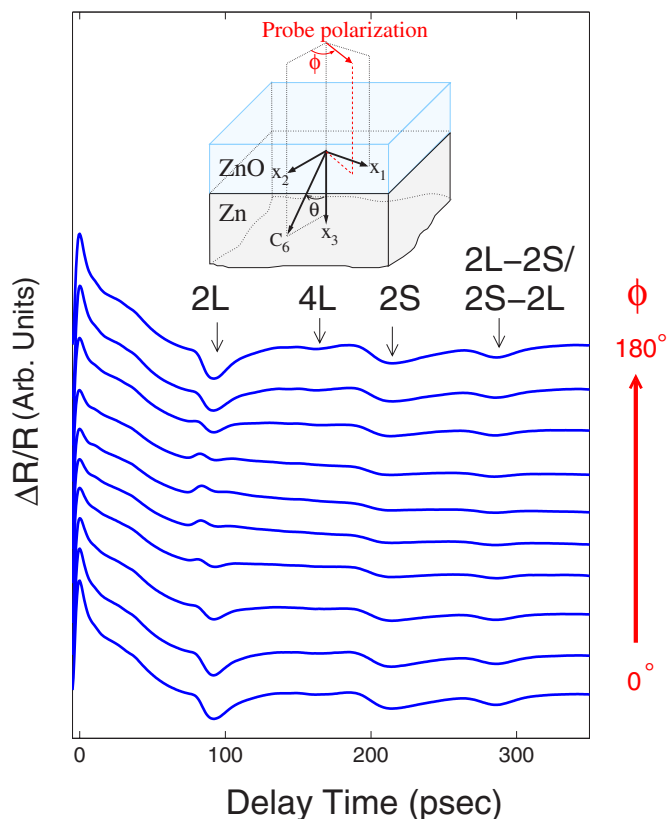


FIG. 4. (Color online) Change in transient reflectivity as a function of probe polarization for a Zn single-crystal substrate with  $C_6$  axis oriented at an angle  $\theta \sim 36^\circ$  relative to the interface normal and on which a transparent ZnO film of 270 nm thickness is deposited.

### III. THERMOELASTIC GENERATION IN ANISOTROPIC OPAQUE MEDIUM

To the best of our knowledge, the first formulation of the problem of efficiency of the thermoelastic excitation of sound in anisotropic materials was proposed 20 years ago.<sup>22</sup> However, only the generation efficiency of the longitudinal waves propagating along the directions of high symmetry was analyzed, while the anisotropy of the thermal expansion was not taken into account. Later on, a numerical model<sup>23</sup> was developed for the description of the thermoelastic generation of the acoustic waves of different polarizations in an orthotropic medium. The model<sup>23</sup> deals with the anisotropy of thermal expansion. However, the analysis was undertaken in a geometry with unbroken symmetry (the crystal surface is oriented perpendicularly to one of the crystallographic axes). In this case, plane acoustic waves with shear components propagating from the laser irradiated surface are not excited. Recently, the thermoelastic excitation of acoustic waves near the free surface of an anisotropic media was revisited using the method of images<sup>24</sup> and the method of integral transforms.<sup>25</sup>

In the present paper, we extend the theory of thermoelastic generation of acoustic waves by lasers in anisotropic materials<sup>25</sup> to the case of current experimental interest: an isotropic transparent film deposited on a semi-infinite opaque disoriented crystal (see Fig. 5). The problem can be further

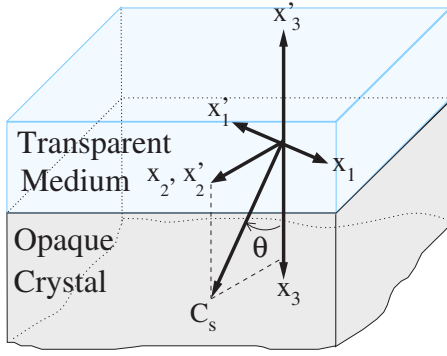


FIG. 5. (Color online) Assumed geometry for the theoretical analysis of the thermoelastic generation of the acoustic waves. The photoelastic process occurs beneath the interface of the semi-infinite anisotropic opaque crystal coated by a transparent isotropic film, considered as semi-infinite as well.

simplified by taking into account that in our experiments the spatial extent of the ultrashort acoustic pulses is shorter than the film thickness. Consequently, in the analysis of the thermoelastic generation process, we will consider the transparent medium as semi-infinite.

### A. General theory

The starting point of the thermoelastic theory are the equations of motion in both media, that is, in the transparent isotropic film (F) and the opaque anisotropic substrate (S),

$$\rho^* \frac{\partial^2 u_i^*}{\partial t^2} = \frac{\partial \sigma_{i3}^*}{\partial x_3^*}, \quad (3)$$

where  $\rho^*$  is the mass density,  $u_i^*$  is the acoustic displacement, and  $\sigma_{ij}^*$  is the stress defined by

$$\sigma_{i3}^* = C_{i3k3}^* S_{k3}^* - B_{i3}^* T^*, \quad S_{k3}^* = \frac{\partial u_k^*}{\partial x_3^*}. \quad (4)$$

The superscript  $*$  means that the equation is similar for both media S and F (i.e.,  $x_3^*$  is simply  $x_3$  for medium S and  $x_3'$  for medium F, respectively). The Einstein summation convention is implicit throughout this paper [i.e., in Eq. (4), the summation is done over  $k$  ( $=1, 2, \text{ and } 3$ ) for a given  $i$ ]. These equations of motion are coupled by the boundary conditions at the interface,

$$\begin{aligned} \sigma_{i3}(x_3 = 0, t) &= (-1)^{i+1} \sigma'_{i3}(x'_3 = 0, t), \\ u_i(x_3 = 0, t) &= (-1)^i u'_i(x'_3 = 0, t). \end{aligned} \quad (5)$$

The coefficients  $(-1)^{i+1}$  and  $(-1)^i$  appear due to the axis convention shown in Fig. 5. The elastic stiffness tensor  $C_{ijkl}^*$  and the thermoelastic stress tensor  $B_{ij}^*$  are expressed in the coordinate axes represented in Fig. 5 that have an arbitrary orientation relative to the crystal axes. As already discussed

in the Introduction, those equations assume a one-dimensional source where all the parameters depend on the  $x_3^*$  spatial coordinate only.

The heat diffusion equations that satisfy

$$\frac{\partial T}{\partial t} = \chi_{33} \frac{\partial^2 T}{\partial x_3^2} + \frac{\alpha I}{\rho c_p} f(t) e^{-\alpha x_3}, \quad (6)$$

$$\frac{\partial T'}{\partial t} = \chi'_{33} \frac{\partial^2 T'}{\partial x_3'^2} \quad (7)$$

govern the thermoelastic stress  $-B_{i3}^* T^*$  of Eq. (4). Here,  $\chi_{33}$  and  $\chi'_{33}$  are the thermal diffusivities in the  $x_3^*$  direction of S and F media, respectively,  $c_p$  is the specific heat, and  $\alpha$  is the optical absorption coefficient of S. The intensity  $I$  is the effective intensity that reaches the opaque crystal for an incident laser radiation of temporal profile  $f(t)$ . The temperature boundary conditions couple Eqs. (6) and (7),

$$\chi_{33} \frac{\partial T}{\partial x_3}(x_3 = 0, t) = -\chi'_{33} \frac{\partial T'}{\partial x_3'}(x'_3 = 0, t).$$

$$T(x_3 = 0, t) = T'(x'_3 = 0, t). \quad (8)$$

The general solution procedure consists of applying temporal  $t$ -Fourier and spatial  $x_3^*$ -Laplace transformations, as defined by

$$\tilde{u}_i^*(x_3^*, \omega) = \int_{-\infty}^{+\infty} u_i^*(x_3^*, t) e^{j\omega t} dt, \quad (9)$$

$$\hat{u}_i^*(p, \omega) = \int_0^{+\infty} \tilde{u}_i^*(x_3^*, \omega) e^{-px_3^*} dx_3^*, \quad (10)$$

to the whole set of equations (3)–(8). Here,  $\tilde{u}_i^*$  is the  $t$ -Fourier transform of  $u_i^*$  and  $\hat{u}_i^*$  the  $x_3^*$ -Laplace transform of  $\tilde{u}_i^*$ ,  $p$  is a complex variable,  $\omega$  is a real variable, and  $j^2 = -1$ . We recall that  $x_3^*$  must be replaced by  $x_3'$  and  $x_3$  when the above transformations concern the media F and S, respectively.

Following this procedure, the transformed equation of motion (3) can be written in the form

$$\begin{aligned} -\rho^* \omega^2 \hat{u}_i^* &= C_{i3k3}^* \left[ p^2 \hat{u}_k^* - p \tilde{u}_k^*(0, \omega) - \frac{\partial \tilde{u}_k^*}{\partial x_3^*}(0, \omega) \right] - p B_{i3}^* \hat{T}^* \\ &+ B_{i3}^* \tilde{T}^*(0, \omega). \end{aligned} \quad (11)$$

The  $t$ -Fourier transformation of the stress that appears in Eq. (4), at the specific coordinate  $x_3^* = 0$ ,

$$\tilde{\sigma}_{i3}^*(0, \omega) = C_{i3k3}^* \frac{\partial \tilde{u}_k^*}{\partial x_3^*}(0, \omega) - B_{i3}^* \tilde{T}^*(0, \omega), \quad (12)$$

allows a simplification of Eq. (11) that can be rewritten as follows:

$$-\rho^* \omega^2 \hat{u}_i^* = C_{i3k3}^* [p^2 \hat{u}_k^* - p \tilde{u}_k^*(0, \omega)] - p B_{i3}^* \hat{T}^* - \tilde{\sigma}_{i3}^*(0, \omega). \quad (13)$$

Equation (13) can be simplified as

$$P_{ij}^* \hat{u}_j^* = S_i^*, \quad (14)$$

where the matrix  $P_{ij}^*$  satisfies

$$P_{ij}^* = p^2 C_{i3j3}^* + \rho^* \omega^2 \delta_{ij}, \quad (15)$$

and  $\delta_{ij}$  is the Kronecker function. The vector  $S_i^*$  verifies

$$S_i^* = p \phi_{i3}^*(p, \omega) + \tilde{\sigma}_{i3}^*(0, \omega), \quad (16)$$

where

$$\phi_{i3}^*(p, \omega) = C_{i3k3}^* \tilde{u}_k^*(0, \omega) + B_{i3}^* \hat{T}^*(p, \omega). \quad (17)$$

Following the detailed method described in Ref. 25 that requires the use of the Cramer determinant technique, the system (14) gives the transformed acoustic displacements,

$$\hat{u}_i^*(p, \omega) = \Delta_i^*(p, \omega) / \Delta^*, \quad (18)$$

where  $\Delta^* = \det(P_{ij}^*)$  is the Cramer determinant and  $\Delta_i^*(p, \omega)$  can be written in the form

$$\Delta_i^*(p, \omega) = p^5 \{ a_{ij}^*(p, \omega) [\phi_{j3}^*(p, \omega) + \tilde{\sigma}_{j3}^*(0, \omega)] / p \}. \quad (19)$$

The symmetrical  $a_{ij}^*(p, \omega)$  coefficients satisfy

$$a_{11}^*(p, \omega) = \left( C_{44}^* + \frac{\rho^* \omega^2}{p^2} \right) \left( C_{33}^* + \frac{\rho^* \omega^2}{p^2} \right) - C_{34}^{*2},$$

$$a_{22}^*(p, \omega) = \left( C_{55}^* + \frac{\rho^* \omega^2}{p^2} \right) \left( C_{33}^* + \frac{\rho^* \omega^2}{p^2} \right) - C_{35}^{*2},$$

$$a_{33}^*(p, \omega) = \left( C_{55}^* + \frac{\rho^* \omega^2}{p^2} \right) \left( C_{44}^* + \frac{\rho^* \omega^2}{p^2} \right) - C_{45}^{*2},$$

$$a_{12}^*(p, \omega) = C_{35}^* C_{34}^* - C_{45}^* \left( C_{33}^* + \frac{\rho^* \omega^2}{p^2} \right),$$

$$a_{13}^*(p, \omega) = C_{45}^* C_{43}^* - C_{35}^* \left( C_{44}^* + \frac{\rho^* \omega^2}{p^2} \right),$$

$$a_{23}^*(p, \omega) = C_{35}^* C_{45}^* - C_{34}^* \left( C_{55}^* + \frac{\rho^* \omega^2}{p^2} \right). \quad (20)$$

Contracted notation is used for the symmetrical elastic stiffness tensor  $C_{ijkl}$ . The six roots  $\pm j k_i^*$  of the Cramer determinant  $\Delta^*$  are reminiscent of the three acoustic mode wave numbers  $k_i^*$ . Inverse Laplace transformation of Eq. (18) is achieved by evaluating the residues of the six roots  $\pm j k_i^*$ . The outcome of this procedure is an expression for the acoustic displacements  $\tilde{u}_i^*(x_3, \omega)$  in the Fourier domain,

$$\begin{aligned} \tilde{u}_i^*(x_3, \omega) = \sum_{r=1}^6 R_{r,i}^* = & \frac{\Delta_i^*(j k_1^*, \omega) e^{j k_1^* x_3}}{2 j k_1^* a^*(k_1^{*2} - k_2^{*2})(k_1^{*2} - k_3^{*2})} \\ & + \frac{\Delta_i^*(-j k_1^*, \omega) e^{-j k_1^* x_3}}{-2 j k_1^* a^*(k_1^{*2} - k_2^{*2})(k_1^{*2} - k_3^{*2})} \\ & + \frac{\Delta_i^*(j k_2^*, \omega) e^{j k_2^* x_3}}{2 j k_2^* a^*(k_2^{*2} - k_1^{*2})(k_2^{*2} - k_3^{*2})} \\ & + \frac{\Delta_i^*(-j k_2^*, \omega) e^{-j k_2^* x_3}}{-2 j k_2^* a^*(k_2^{*2} - k_1^{*2})(k_2^{*2} - k_3^{*2})} \\ & + \frac{\Delta_i^*(j k_3^*, \omega) e^{j k_3^* x_3}}{2 j k_3^* a^*(k_3^{*2} - k_1^{*2})(k_3^{*2} - k_2^{*2})} \\ & + \frac{\Delta_i^*(-j k_3^*, \omega) e^{-j k_3^* x_3}}{-2 j k_3^* a^*(k_3^{*2} - k_1^{*2})(k_3^{*2} - k_2^{*2})}, \quad (21) \end{aligned}$$

where  $R_{r,i}^*$  are the six residues corresponding to the wave numbers  $\pm k_i^*$ , and the coefficient  $a^*$  depends on the elastic stiffness coefficients,

$$a^* = C_{55}^* C_{44}^* C_{33}^* - C_{55}^* C_{34}^{*2} - C_{44}^* C_{35}^{*2} - C_{33}^* C_{45}^{*2} + 2 C_{45}^* C_{34}^* C_{35}^*. \quad (22)$$

The inverse Fourier transform of Eq. (21) will provide the general spatiotemporal solutions of the displacements  $u_i^*(x_3, t)$ , valid outside the area of excitation. Equation (21) involves two kinds of waves with wave number  $\pm k_i^*$ . Concretely, each exponent  $e^{j k_i^* x_3}$  of Eq. (21) is a wave coming from the interface and each exponent  $e^{-j k_i^* x_3}$  of Eq. (21) is a wave coming from infinity. Noting that the wave coming from infinity is unphysical, we obtain the following conditions on the determinant  $\Delta_i^*(p, \omega)$  at the specific values of  $p = -j k_i^*$ :

$$\Delta_i^*(-j k_1^*, \omega) = \Delta_i^*(-j k_2^*, \omega) = \Delta_i^*(-j k_3^*, \omega) = 0. \quad (23)$$

Finally, the general expression for the acoustic displacement in the Fourier domain far from the laser excited area can be expressed in the form

$$\begin{aligned} \tilde{u}_i^*(x_3, \omega) = & \frac{\Delta_i^*(j k_1^*, \omega) e^{j k_1^* x_3}}{2 j k_1^* a^*(k_1^{*2} - k_2^{*2})(k_1^{*2} - k_3^{*2})} \\ & + \frac{\Delta_i^*(j k_2^*, \omega) e^{j k_2^* x_3}}{2 j k_2^* a^*(k_2^{*2} - k_1^{*2})(k_2^{*2} - k_3^{*2})} \\ & + \frac{\Delta_i^*(j k_3^*, \omega) e^{j k_3^* x_3}}{2 j k_3^* a^*(k_3^{*2} - k_1^{*2})(k_3^{*2} - k_2^{*2})}. \quad (24) \end{aligned}$$

Each coefficient  $\Delta_i^*(j k_r^*, \omega)$  of Eq. (24) is coupled to the unknowns  $\tilde{u}_i^*(0, \omega)$ ,  $\tilde{\sigma}_i^*(0, \omega)$ , and  $\hat{T}^*(j k_r^*, \omega)$  through Eqs. (17) and (19). Hence, the next step in the solution consists in obtaining analytical expression for each coefficient  $\Delta_i^*(j k_r^*, \omega)$  of Eq. (24), in order to derive these unknowns. This task can be straightforwardly realized by making an approximation concerning the transparent film F that reduces

the complexity of the problem. However, this can be accomplished without additional assumptions when necessary.

### B. Simplified problem

Since at the picosecond time scale thermal diffusion is commonly neglected in the thermoelastic generation process (even in a metallic medium such as substrate S), it follows that in the transparent dielectric medium F, the thermal diffusion contribution can be neglected with even more accuracy. That is, in the following we will neglect the thermal diffusion contribution and correspondingly we will assume that the temperature rise  $T'$  induced in the transparent film F due to the heat diffusion from the absorptive crystal S is negligible. Note that this contribution could have played a role in the case of an anomalously high thermoelastic modulus tensor  $B'_{ij}$  of the film, but this is not the situation in our case.

The above approximation leads to a modification of Eq. (24) that is operationally faster and easier to obtain by applying the inverse Laplace transform of Eq. (13) than by developing the coefficients  $\Delta'_i(jk'_r, \omega)$  of Eq. (24). In fact, by neglecting thermal diffusion, Eq. (13) becomes

$$\hat{u}'_i(p, \omega) = \frac{pC'_{i3i3}\tilde{u}'_i(0, \omega) + \tilde{\sigma}'_{i3}(0, \omega)}{p^2C'_{i3i3} + \rho'\omega^2}. \quad (25)$$

We recall that the prime index means that the equations deal with the isotropic film F. Then, the inverse Laplace transform of Eq. (25), performed using the technique of the calculus of residues, provides the solution for the displacement in the frequency domain,

$$\begin{aligned} \tilde{u}'_i(x'_3, \omega) = & \frac{jk'_i C'_{i3i3} \tilde{u}'_i(0, \omega) - \tilde{\sigma}'_{i3}(0, \omega)}{2jk'_i C'_{i3i3}} e^{jk'_i x'_3} \\ & + \frac{(-jk'_i C'_{i3i3} \tilde{u}'_i(0, \omega) + \tilde{\sigma}'_{i3}(0, \omega))}{-2jk'_i C'_{i3i3}} e^{-jk'_i x'_3}. \end{aligned} \quad (26)$$

As mentioned previously, the solutions (26) are only valid outside the area of thermoelastic excitation. In that sense, the second term of Eq. (26) that corresponds to waves coming from infinity is physically inappropriate, and thus must be zero,

$$jk'_i C'_{i3i3} \tilde{u}'_i(0, \omega) = -\tilde{\sigma}'_{i3}(0, \omega). \quad (27)$$

Finally, Eq. (27) allows a simplification of Eq. (26),

$$\tilde{u}'_i(x'_3, \omega) = \tilde{u}'_i(0, \omega) e^{jk'_i x'_3}. \quad (28)$$

This last equation highlights the fact that by neglecting the thermal diffusion in the transparent film F, the displacements at the interface  $\tilde{u}'_i(0, \omega)$  govern the excitation of the acoustic waves inside the film. Thus, the unknowns  $\tilde{u}'_i(0, \omega)$  are the key to this problem.

Hence, the next step of the solution consists in getting the transformed boundary acoustic displacements  $\tilde{u}'_i(0, \omega) = (-1)^i \tilde{u}_i(0, \omega)$ . This is realized by analyzing the Eqs. (23) that involve the acoustic displacements at the interface. Among the nine equations that are expressed by Eqs. (23), a

relevant set of three equations involving the three unknowns,  $\tilde{u}_i(0, \omega)$ , can be written in the form

$$\begin{aligned} \rho v_i^2 a_{ij}(v_i) \tilde{u}_i(0, \omega) = & -a_{ir}(v_1) B_{r3} \hat{T}(-jk_i, \omega) \\ & + a_{ir}(v_i) \tilde{\sigma}_{r3}(0, \omega) / jk_i. \end{aligned} \quad (29)$$

Concerning the transparent medium F, transposition of the last set of equations (29) leads to the previous equation (27). The Fourier transformed boundary conditions of the stresses,  $\tilde{\sigma}'_{i3}(0, \omega) = (-1)^{i+1} \tilde{\sigma}_{i3}(0, \omega)$  and of the acoustic displacements  $\tilde{u}'_i = (-1)^i \tilde{u}_i$ , with the axes conventions of Fig. 5, provide the following system from Eqs. (27) and (29):

$$A_{ij} \tilde{u}_i(0, \omega) = -a_{ir}(v_i) B_{r3} \hat{T}(-jk_i, \omega), \quad (30)$$

where

$$A_{ij} = (\rho v_i^2 + \rho' v_i v'_j) a_{ij}(v_i). \quad (31)$$

The solutions  $\tilde{u}_i(0, \omega)$  of Eq. (30) are deduced using the Cramer technique in the form

$$\tilde{u}_i(0, \omega) = \beta_{im} \hat{T}(-jk_m, \omega). \quad (32)$$

The  $\beta_{im}$  coefficients are deduced from the quotient of the Cramer determinants of the system (30) (they do not depend on the frequency  $\omega$ ),

$$\begin{aligned} \beta_{11} = & -a_{1r}(v_1) B_{r3} [(\rho v_2^2 + \rho' v_2 v'_2) \\ & \times (\rho v_3^2 + \rho' v_3 v'_3) a_{22}(v_2) a_{33}(v_3) \\ & - (\rho v_3^2 + \rho' v_3 v'_2)(\rho v_2^2 + \rho' v_2 v'_3) \\ & \times a_{23}(v_3) a_{23}(v_2)] / \det(A_{ij}), \end{aligned}$$

$$\begin{aligned} \beta_{12} = & a_{2r}(v_2) B_{r3} [(\rho v_1^2 + \rho' v_1 v'_2) \\ & \times (\rho v_3^2 + \rho' v_3 v'_3) a_{12}(v_1) a_{33}(v_3) \\ & - (\rho v_3^2 + \rho' v_3 v'_2)(\rho v_1^2 + \rho' v_1 v'_3) \\ & \times a_{23}(v_3) a_{13}(v_1)] / \det(A_{ij}), \end{aligned}$$

$$\begin{aligned} \beta_{13} = & -a_{3r}(v_3) B_{r3} [(\rho v_1^2 + \rho' v_1 v'_2) \\ & \times (\rho v_2^2 + \rho' v_2 v'_3) a_{12}(v_1) a_{23}(v_2) \\ & - (\rho v_2^2 + \rho' v_2 v'_2)(\rho v_1^2 + \rho' v_1 v'_3) \\ & \times a_{22}(v_2) a_{13}(v_1)] / \det(A_{ij}), \end{aligned}$$

$$\begin{aligned} \beta_{21} = & a_{1r}(v_1) B_{r3} [(\rho v_2^2 + \rho' v_2 v'_1) \\ & \times (\rho v_3^2 + \rho' v_3 v'_3) a_{12}(v_2) a_{33}(v_3) \\ & - (\rho v_3^2 + \rho' v_3 v'_1)(\rho v_2^2 + \rho' v_2 v'_3) \\ & \times a_{13}(v_3) a_{23}(v_2)] / \det(A_{ij}), \end{aligned}$$

$$\begin{aligned} \beta_{22} = & -a_{2r}(v_2) B_{r3} [(\rho v_1^2 + \rho' v_1 v'_1) \\ & \times (\rho v_3^2 + \rho' v_3 v'_3) a_{11}(v_1) a_{33}(v_3) \\ & - (\rho v_1^2 + \rho' v_1 v'_3)(\rho v_3^2 + \rho' v_3 v'_1) \\ & \times a_{13}(v_1) a_{13}(v_3)] / \det(A_{ij}), \end{aligned}$$

$$\begin{aligned} \beta_{23} = & a_{3r}(v_3)B_{r3}[(\rho v_1^2 + \rho'v_1v_1') \\ & \times (\rho v_2^2 + \rho'v_2v_2')a_{11}(v_1)a_{23}(v_2) \\ & - (\rho v_2^2 + \rho'v_2v_2')(\rho v_1^2 + \rho'v_1v_1') \\ & \times a_{12}(v_2)a_{13}(v_1)]/\det(A_{ij}), \end{aligned}$$

$$\begin{aligned} \beta_{31} = & -a_{1r}(v_1)B_{r3}[(\rho v_2^2 + \rho'v_2v_2') \\ & \times (\rho v_3^2 + \rho'v_3v_3')a_{12}(v_2)a_{23}(v_3) \\ & - (\rho v_3^2 + \rho'v_3v_3')(\rho v_2^2 + \rho'v_2v_2')a_{13}(v_3) \\ & \times a_{22}(v_2)]/\det(A_{ij}), \end{aligned}$$

$$\begin{aligned} \beta_{32} = & a_{2r}(v_2)B_{r3}[(\rho v_1^2 + \rho'v_1v_1') \\ & \times (\rho v_3^2 + \rho'v_3v_3')a_{11}(v_1)a_{23}(v_3) \\ & - (\rho v_1^2 + \rho'v_1v_1')(\rho v_3^2 + \rho'v_3v_3') \\ & \times a_{12}(v_1)a_{13}(v_3)]/\det(A_{ij}), \end{aligned}$$

$$\begin{aligned} \beta_{33} = & -a_{3r}(v_3)B_{r3}[(\rho v_1^2 + \rho'v_1v_1') \\ & \times (\rho v_2^2 + \rho'v_2v_2')a_{11}(v_1)a_{22}(v_2) \\ & - (\rho v_1^2 + \rho'v_1v_1')(\rho v_2^2 + \rho'v_2v_2') \\ & \times a_{12}(v_1)a_{12}(v_2)]/\det(A_{ij}). \end{aligned} \quad (33)$$

The Fourier-transformed solutions in the transparent medium are then deduced from Eq. (28),

$$\tilde{u}'_i(x'_3, \omega) = (-1)^i \beta_{im} \hat{T}(-jk_m, \omega) e^{jk'_i x'_3}. \quad (34)$$

In order to obtain the spatiotemporal solutions of the displacements, the inverse Fourier transform of  $\hat{T}(-jk_m, \omega)$  must be performed in Eq. (34). The general expression of  $\hat{T}(-jk_m, \omega)$ , whose inverse Fourier transform can be fully analytically treated, is detailed in the Ref. 25. To further reduce the complexity of the problem, it is again possible to neglect thermal diffusion even in the substrate S. This simplification facilitates the inverse Fourier transformation of  $\hat{T}(-jk_m, \omega)$ . Finally, we obtain

$$u'_i(x'_3, t) = (-1)^i \left( \frac{F}{\rho c_p} \right) \beta_{im} (1 - e^{-\alpha v_m (t - x'_3/v'_i)}), \quad (35)$$

for  $t - \frac{x'_3}{v'_i} \geq 0$ , and

$$u'_i(x'_3, t) = 0, \quad (36)$$

for  $t - \frac{x'_3}{v'_i} < 0$ , where  $F$  is the laser fluence,  $\rho$  is the mass density, and  $c_p$  is the specific heat. The corresponding strain is deduced from Eqs. (35) and (36),

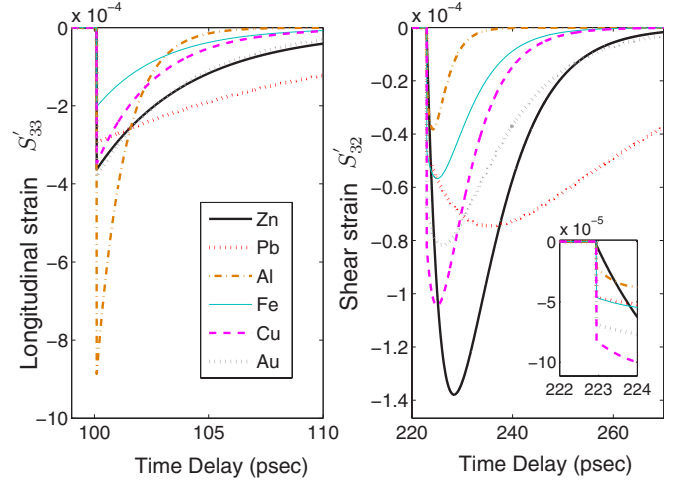


FIG. 6. (Color online) Dynamics of the longitudinal  $S'_{33}$  and shear  $S'_{32}$  strains at an arbitrarily chosen coordinate  $x'_3=610$  nm inside a ZnO semi-infinite transparent medium F on top of a semi-infinite metallic crystal S, of different kinds, each with a cut off-axis of symmetry by  $\theta=28^\circ$ . The laser fluence value is  $F_L=1$  J m $^{-2}$ . Both thermal and electronic diffusions are neglected.

$$S'_{3i}(x'_3, t) = (-1)^{i+1} \left( \frac{\alpha F}{\rho c_p} \right) \frac{v_m}{v'_i} \beta_{im} e^{-\alpha v_m (t - x'_3/v'_i)}, \quad (37)$$

for  $t - \frac{x'_3}{v'_i} < 0$ , and

$$S'_{3i}(x'_3, t) = 0, \quad (38)$$

for  $t - \frac{x'_3}{v'_i} > 0$ . The physical meaning of the  $\beta_{im}$  coefficients is clear from Eqs. (37): they weight the contribution of each individual acoustic mode, i.e.,  $\beta_{im}$  weights the contribution of the  $m$ th thermoelastically excited acoustic modes of the crystal S to the  $i$ th acoustic mode of the transparent medium F.

### C. Asynchronous mechanism of shear generation

In this section, we will describe the asynchronous mechanism of shear generation that is revealed by a careful analysis of the above thermoelastic generation theory. To this end, we present the results of the computation of the shear strain generated for various crystals. All the parameters necessary to perform the simulations were found in Refs. 26 and 27. Regarding the symmetry induced by the  $\theta$  tilt of the symmetry axis  $C_6$  (see Fig. 5), the purely transverse mode  $S'_{31}$ , whose acoustic displacement  $u'_1$  is pointing in the  $x_1$  direction, cannot be excited in any kind of the considered crystals S. Consequently, only four nonzero  $\beta_{im}$  coefficients are considered,  $\beta_{22}$ ,  $\beta_{23}$ ,  $\beta_{32}$ , and  $\beta_{33}$ . The coefficients  $\beta_{22}$  and  $\beta_{32}$  correspond to the contribution of the quasishear (QS) mode, and  $\beta_{23}$  and  $\beta_{33}$  to that of the quasilongitudinal (QL) mode excited in the disoriented crystal S. Figure 6 shows the simulation of the dynamics of the longitudinal  $S'_{33}$  and the shear  $S'_{32}$  strains recorded at some coordinate  $x'_3=610$  nm inside the ZnO transparent medium F (assumed to be semi-infinite), for different kinds of metallic disoriented crystals of cubic symmetry (Pb, Al, Fe, Cu, and Au) and of hexagonal sym-

metry (Zn). The tilt angle  $\theta$  around  $28^\circ$  corresponds to the optimum for shear strain generation in all crystals. After the delayed times since laser action of  $\tau_{33}=100$  ps and  $\tau_{32}=223$  ps, corresponding to a travel time inside the ZnO film at two different velocities of  $v'_3=6096$  m s $^{-1}$  and  $v'_2=2736$  m s $^{-1}$ , the longitudinal and the shear strains arrive at the chosen coordinate  $x'_3=610$  nm.

First of all, these numerical simulations provide clear evidence that the shear acoustic generation efficiency is comparable with that of the longitudinal-acoustic generation.<sup>28</sup> Moreover, they attest that shear generation is possible even in cubic disoriented crystals S whose thermal dilatation tensor  $\beta_{ij}^T$  and static strain tensor  $S_{ij}^T=\beta_{ij}^T T$  are spherical. Additionally, these calculations highlight a strong difference in the shape of each strain field that cannot be explained by classic approach of the thermoelastic generation theory.<sup>4</sup> Indeed, the shear strain field exhibits a temporal duration of the leading front subsequently broader as well as a clear difference in the leading-front shape than for the longitudinal strain field (see Fig. 6). In addition, just at the moment the strain field arrives (which corresponds for the longitudinal and the shear strains displayed in Fig. 6 to delays of  $\tau_L \sim 100$  ps and  $\tau_S \sim 223$  ps, respectively), the longitudinal strain is maximum, in contrast with the shear strain, which is minimum. This unexpected behavior reveals that the longitudinal strain excitation takes place in the very early stages of the laser thermoelastic excitation, while the shear strain excitation requires some delay (i.e., the shear strain starts almost from zero and its maximum is shifted by a few picoseconds). All these features are consistent with our experimental observations since the difference in both the strength and the leading front are observed (see Fig. 3). This shear strain excitation peculiarity, never before reported, finds its origin in the so-called asynchronous mechanism of shear generation, as explained below.

As already mentioned in the Introduction, the shear strain  $S'_{23}$  transmitted in the film F is the result of the contributions of the quasimodes QL and QS of the crystal S, each of which carries an exponential strain profile given by the exponential depth profile of the laser excitation,

$$S_{23}^{QL}(0,t) \sim \exp(-\alpha v_3 t), \quad S_{23}^{QS}(0,t) \sim \exp(-\alpha v_2 t), \quad (39)$$

where  $v_3$  and  $v_2$  are the velocities of the QL and QS acoustic modes of the crystal, and  $S_{23}^{QL}(0,t)$  and  $S_{23}^{QS}(0,t)$  are the shear strain contributions of the QL and QS acoustic modes, respectively, at the interface  $x_3=x'_3=0$ . While the total longitudinal strain  $S_{33}$  induced in the crystal is greatest at  $t=0$  (i.e., the longitudinal strain carries the summation of two positive exponents), in the general case of spherical dilatation tensor, the total shear strain at  $t=0$  is a summation of two exponents of opposite signs,

$$S_{23}(0,t) = S_{23}^{QS}(0,t) - S_{23}^{QL}(0,t) \\ \sim [\exp(-\alpha v_2 t) - \exp(-\alpha v_3 t)]H(t), \quad (40)$$

where  $H(t)$  is the Heaviside function. As a consequence, due to the exact compensation of the individual shear strain contributions of the quasimodes excited in the crystal S with

spherical thermal dilatation, the total shear strain is canceled at  $t=0$ . However, thanks to the mismatch propagation of the modes QL and QT in the direction of the interface, the separation of the shear strain contributions happens and reaches a maximum for a time defined by

$$\delta t = \frac{1}{\alpha(v_3 - v_2)} \ln\left(\frac{v_3}{v_2}\right). \quad (41)$$

This time delay is given by the differentiation with respect to time of the total shear strain (40). It matches the shear strain profile transmitted in the film F and describes the spatial separation of the two shear mode components over the optical area of excitation  $\sim 1/\alpha$ . Concretely, due to the difference between the acoustic velocities  $v_3$  and  $v_2$ , the shear strain increases starting at  $t=0$  (in the early stages, the shear strain excitation is of virtual character) and reaches a maximum at  $t=\delta t$  when the compensation of each individual shear strain mode is minimized. As a consequence, the shear strain front is broadened in comparison with the longitudinal strain front. This is observed in Fig. 6, where the maximum of the shear strain is shifted in accordance with the difference between the acoustic velocities of the quasimodes of each material investigated. The inset of Fig. 6 highlights a non-zero abrupt contribution of the shear strain leading front that is attributed to the surface mediated mode conversion of the initially nonzero longitudinal strain, that have nothing to compare with the asynchronous mechanism of shear generation, without which the shear strain generated would have been of significantly lower amplitude.

In anisotropic crystals, the thermoelastic generation of acoustic waves is governed by the very general properties of the thermoelastic stress tensor  $\sigma_{ij}^T = C_{ijkl} \beta_{kl}^T T$  that depend not only on the thermal-expansion tensor  $\beta_{kl}^T$  but also on the elastic stiffness tensor  $C_{ijkl}$ . Consequently, it is not the deviatoric part of  $\beta_{kl}^T$  (which is zero in the case of cubic crystals and nonzero in the specific case of zinc crystal) but rather the deviatoric thermoelastic stress tensor  $\bar{\sigma}_{ij}^T = \sigma_{ij}^T - (\sigma_{kk}^T/3)\delta_{ij}$  that directly drives excitations of shear polarization (i.e.,  $x_2$  polarization). Our simulations show that the contribution of the deviatoric thermoelastic stress tensor  $\bar{\sigma}_{ij}^T = \sigma_{ij}^T - (\sigma_{kk}^T/3)\delta_{ij}$  to the amplitude of the shear pulse emitted from Zn into ZnO is less than 40% of the contribution from the isotropic stress  $(\sigma_{kk}^T/3)\delta_{ij}$ . Indeed, the isotropic thermoelastic stress  $(\sigma_{kk}^T/3)\delta_{ij}$  is able to excite shear polarizations as well because of the specific elastic anisotropy of broken symmetry and the asynchronous shear generation mechanism. Although thermoelastic stress  $(\sigma_{kk}^T/3)\delta_{ij}$  locally excites only longitudinal polarizations (i.e.,  $x_3$  polarization) in crystals, the corresponding longitudinal strain is distributed between the longitudinal components of QL and quasi transverse (QT) modes that also contain plane shear strain components, which are initially mutually compensated but later appear because of the asynchronous propagation.

#### IV. THEORY OF DETECTION OF ACOUSTIC WAVES

Owing to the fact that the interferometric detection techniques for shear displacements, previously performed with

nanosecond lasers,<sup>29,30</sup> have never been transposed to the detection of picosecond shear displacements, we experimentally and theoretically investigated the possibility of detecting picosecond shear phonons by the use of the reflectometric technique. This detection technique is sensitive to any phenomenon that modifies the optical properties of the material. For instance, the photoelastic interaction produced by a shear strain that induces a modification in the dielectric tensor can be detected in this manner. In addition, the uncommon behavior of the recorded profile of the echoes within the probe polarization orientation (see Fig. 3) revealed a shortcoming in the theoretical description of the reflectometric detection process in an opaque disoriented crystal. The following theoretical approach describes the reflectometric detection of picosecond shear and longitudinal-acoustic strains in a medium such as a semitransparent or opaque crystal in a geometry with broken symmetry.

Several previous works have treated the theory of reflectometric detection in laser ultrasonics. The theory of reflectometric detection in a semi-infinite opaque isotropic medium has been established for picosecond longitudinal-acoustic strains only.<sup>4,31</sup> Several other theoretical studies<sup>32–34</sup> have been extended to shear picosecond wave detection but still for isotropic medium. The theoretical problem investigated in this part consists in solving the electromagnetic wave propagation in the opaque disoriented medium S perturbed by an acoustic field composed of a combination of several strain fields (resulting from the interface mediated mode conversion of the longitudinal or shear strain waves coming from the isotropic transparent film, decomposed into the quasimodes QL and QS by crossing the crystal interface).

The coupling between the acoustic and the electromagnetic fields is described in Sec. IV B through the linear photoelastic effect. Solution by a first-order perturbation technique is performed in Sec. IV C. The classical electromagnetic boundary conditions are finally applied in Sec. IV D to obtain the general theoretical transient reflectivity coefficient  $\Delta R$ , described in Sec. IV E, required to simulate the experimental measurements.

### A. Electromagnetic wave propagation analysis

Consider the situation of a semi-infinite homogeneous anisotropic medium (called S medium in the previous part) of relative dielectric tensor  $[\epsilon]$  in the  $x_3 > 0$  region. The spatiotemporal modulation of the dielectric tensor induced by the propagating plane acoustic strain through photoelastic effect is described by  $[\delta\epsilon](x_3, t)$  Nelson and Lax perturbed dielectric tensor, and general electromagnetic wave equation for the electric field is then given by

$$\left[ \Delta - \vec{\nabla} \cdot \nabla + \frac{\omega^2}{c^2} ([\epsilon] + [\delta\epsilon]) \right] \vec{E} = \vec{0}. \quad (42)$$

The perturbed dielectric tensor is nonstationary and nonhomogeneous, as it follows the acoustic wave. Because of the relatively low frequency of the acoustic perturbation ( $< 1$  THz) compared with the frequency of the probe light, we can consider the problem as a quasistatic one. Under this

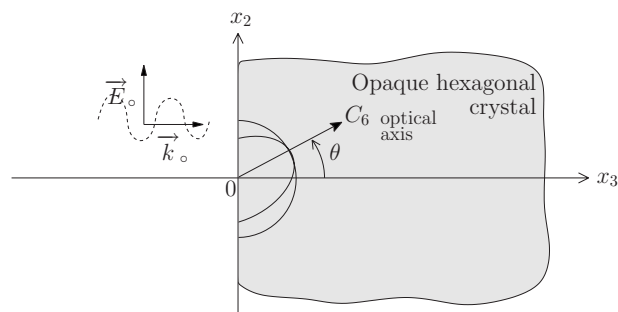


FIG. 7. The probe light is assumed to be normally incident to the crystal surface.

assumption, the perturbed dielectric tensor depends only on the  $x_3$  coordinate,  $[\delta\epsilon](x_3)$ .

For the convenience of the analytical solution of Eq. (42), and in agreement with the experimental protocol, we assume that the probe light is normally incident on the sample surface (Fig. 7). Then, Eq. (42) can be written in the form

$$\frac{\partial^2 E_1}{\partial x_3^2} + \frac{\omega^2}{c^2} (\epsilon_{1i} + \delta\epsilon_{1i}) E_i = 0, \quad (43)$$

$$\frac{\partial^2 E_2}{\partial x_3^2} + \frac{\omega^2}{c^2} (\epsilon_{2i} + \delta\epsilon_{2i}) E_i = 0, \quad (44)$$

$$\frac{\omega^2}{c^2} (\epsilon_{3i} + \delta\epsilon_{3i}) E_i = 0, \quad (45)$$

where  $E_i$  is the  $i$ th component of the electric field, and the summation is done over  $i=1, 2$ , and  $3$ . A common technique used to solve this coupled system of equations consists in applying a perturbative method. In fact, the electric field  $E_i$  solution of the set of equations (43)–(45) can be seen as the superposition of the zero-order electric field  $E_{i,0}$ , i.e., the solution without any perturbation, and the scattered electric fields of increasing orders when the perturbation is taken into account. Concretely, the picosecond strain of  $\sim 10^{-6}$ – $10^{-4}$  of magnitude induces a dielectric perturbation at the same order of magnitude, which allows us to truncate the expansion at first order. In other words, the solution is well described by the following assumption:

$$E_i \sim E_{i,0} + E_{i,1}, \quad (46)$$

where  $E_{i,0}$ , called the zero-order electric field, is the existing electric field when no acoustic perturbation exists in the probed medium.  $E_{i,1}$ , called the first-order electric field, is the additional perturbation term originating from the acoustic disturbance.

In the specific case under investigation of a hexagonal crystal with broken symmetry, the zero-order solutions  $E_{i,0}$  of the set of equations (43)–(45) are well known and can be written in the form

$$E_{1,0} = E_{1,0}^o e^{j\omega[t - (n_o/c)x_3]},$$

$$E_{2,0} = E_{2,0}^o e^{j\omega[t - (n_e/c)x_3]},$$

$$E_{3,0} = -(\epsilon_{23}/\epsilon_{33})E_{2,0}^o e^{j\omega[t - (n_e/c)x_3]}, \quad (47)$$

where  $n_o$  is the ordinary index of refraction and  $n_e$  is the extraordinary index of refraction of the medium. The indices of refraction satisfy  $n_o = \sqrt{\epsilon_{11}^o}$  and  $n_e = \sqrt{\epsilon_{11}^o \epsilon_{33}^o / \epsilon_{33}}$ , where  $\epsilon_{33} = \sin^2 \theta \epsilon_{11}^o + \cos^2 \theta \epsilon_{33}^o$ . Also,  $\theta$  angle is the angle between the  $x_3$  axis and the  $C_6$  axis of symmetry (see Figs. 4 and 5). The superscript  $o$  denotes a component expressed in the crystallographic eigenaxis system. The solutions (47) can be easily extended to any crystal of symmetry order lower than the hexagonal one.

To first order, neglecting the second-order terms  $\delta\epsilon_{ij}E_{i,1}$ , and considering Eqs. (46) and (47), the set of equations (43)–(45) can be expressed as follows:

$$\frac{\partial^2 E_{1,1}}{\partial x_3^2} + \frac{\omega^2}{c^2} \epsilon_{11}^o E_{1,1} = -\frac{\omega^2}{c^2} \delta\epsilon_{1i} E_{i,0}, \quad (48)$$

$$\frac{\partial^2 E_{2,1}}{\partial x_3^2} + \frac{\omega^2}{c^2} \epsilon_{22} E_{2,1} + \frac{\omega^2}{c^2} \epsilon_{23} E_{3,1} = -\frac{\omega^2}{c^2} \delta\epsilon_{2i} E_{i,0}, \quad (49)$$

$$\epsilon_{23} E_{2,1} + \epsilon_{33} E_{3,1} = -\delta\epsilon_{3i} E_{i,0}. \quad (50)$$

These coupled equations are solvable when the perturbed Nelson and Lax tensor is written out explicitly as in next section.

### B. Perturbed tensor of Nelson and Lax

This part aims at determining the expression of the perturbed dielectric tensor  $[\delta\epsilon]$  in the situation of broken sym-

metry. In the crystallographic principal-axis system, the perturbed dielectric tensor verifies

$$\delta\epsilon_{ij}^o = -\epsilon_{im}^o \epsilon_{nj}^o P_{mnkl}^o S_{kl}^o, \quad (51)$$

where  $\epsilon_{im}^o$  is the dielectric tensor and  $P_{mnkl}^o$  is the photoelastic tensor of Nelson and Lax.<sup>35</sup> By using the contracted notations, Eq. (51) is expressed as

$$\delta\epsilon_i^o = -[K^o(I)P_{IJ}^o]S_j^o \equiv -(N_{IJ}^o)S_j^o, \quad (52)$$

where  $S_j^o \equiv S_{jj}^o$  for  $j=1,2,3$ ,  $S_j^o \equiv 2S_{ij}^o$  otherwise. The photoelastic tensor  $P_{IJ}^o$  of an  $\frac{6}{m}mm$  hexagonal symmetry medium is given as<sup>36</sup>

$$P_{IJ}^o = \begin{pmatrix} p_{11} & p_{12} & p_{13} & 0 & 0 & 0 \\ p_{12} & p_{11} & p_{13} & 0 & 0 & 0 \\ p_{31} & p_{31} & p_{33} & 0 & 0 & 0 \\ 0 & 0 & 0 & p_{44} & 0 & 0 \\ 0 & 0 & 0 & 0 & p_{44} & 0 \\ 0 & 0 & 0 & 0 & 0 & (p_{11} - p_{12})/2 \end{pmatrix},$$

and the  $K^o$  vector verifies

$$K^o = \begin{pmatrix} (\epsilon_{11}^o)^2 \\ (\epsilon_{11}^o)^2 \\ (\epsilon_{33}^o)^2 \\ \epsilon_{11}^o \epsilon_{33}^o \\ \epsilon_{11}^o \epsilon_{33}^o \\ (\epsilon_{11}^o)^2 \end{pmatrix}. \quad (53)$$

A trivial calculation of the product  $K^o(I)P_{IJ}^o$ , which is similar to a scalar product [i.e., each  $I$  line of the  $P_{IJ}$  matrix is multiplied by the  $K^o(I)$  coefficient], leads to

$$N_{IJ}^o = K^o(I)P_{IJ}^o = \begin{pmatrix} p_{11}(\epsilon_{11}^o)^2 & p_{12}(\epsilon_{11}^o)^2 & p_{13}(\epsilon_{11}^o)^2 & 0 & 0 & 0 \\ p_{12}(\epsilon_{11}^o)^2 & p_{11}(\epsilon_{11}^o)^2 & p_{13}(\epsilon_{11}^o)^2 & 0 & 0 & 0 \\ p_{31}(\epsilon_{33}^o)^2 & p_{31}(\epsilon_{33}^o)^2 & p_{33}(\epsilon_{33}^o)^2 & 0 & 0 & 0 \\ 0 & 0 & 0 & p_{44}\epsilon_{11}^o\epsilon_{33}^o & 0 & 0 \\ 0 & 0 & 0 & 0 & p_{44}\epsilon_{11}^o\epsilon_{33}^o & 0 \\ 0 & 0 & 0 & 0 & 0 & \frac{(p_{11} - p_{12})}{2}(\epsilon_{11}^o)^2 \end{pmatrix}. \quad (54)$$

The contracted formulation (54) corresponds to the conventional situation when the  $C_6$  axis of symmetry coincides with the  $x_3$  axis. Due to the broken symmetry, the tensor (54) has to be transformed by applying the tensorial rules of coordinate changes. Since the only possible acoustic strain fields in the anisotropic medium are  $S_{33} \equiv S_3$  and  $S_{23} \equiv S_4$  (see previous part dealing with thermoelastic generation and also

previous work<sup>25</sup>), the calculation of  $N_{IJ}$  in the situation when the symmetry axis  $C_6$  is tilted from the  $x_3$  axis by an angle  $\theta$  can be restricted to the calculation of the columns  $C_3$  and  $C_4$  of that tensor. That restriction shows then that the columns  $C_3$  and  $C_4$  are the only ones required to obtain the perturbation series and thus the terms of the perturbed dielectric tensor. The columns  $C_3$  and  $C_4$  of the tensor  $N_{IJ}$  satisfy

$$(N_{IJ})_{C_3, C_4} = \begin{pmatrix} (\sin^2 \theta p_{12} + \cos^2 \theta p_{13})(\epsilon_{11}^o)^2 & \cos \theta \sin \theta (p_{13} - p_{12})(\epsilon_{11}^o)^2 \\ [\cos^2 \theta p_{11}(\epsilon_{11}^o)^2 + \sin^2 \theta p_{31}(\epsilon_{r,3}^o)^2] \sin^2 \theta & \cos \theta \sin \theta [\cos^2 \theta (p_{13} - p_{11})(\epsilon_{11}^o)^2 \\ + [\cos^2 \theta p_{13}(\epsilon_{r,1}^o)^2 + \sin^2 \theta p_{33}(\epsilon_{33}^o)^2] \cos^2 \theta & + \sin^2 \theta (p_{33} - p_{31})(\epsilon_{33}^o)^2 \\ - 4 \cos^2 \theta \sin^2 \theta p_{44} \epsilon_{11}^o \epsilon_{33}^o & + 2 p_{44} \epsilon_{11}^o \epsilon_{33}^o \cos 2\theta] \\ [\sin^2 \theta p_{11}(\epsilon_{11}^o)^2 + \cos^2 \theta p_{31}(\epsilon_{33}^o)^2] \sin^2 \theta & \cos \theta \sin \theta [\sin^2 \theta (p_{13} - p_{11})(\epsilon_{11}^o)^2 \\ + [\sin^2 \theta p_{13}(\epsilon_{11}^o)^2 + \cos^2 \theta p_{33}(\epsilon_{33}^o)^2] \cos^2 \theta & + \cos^2 \theta (p_{33} - p_{31})(\epsilon_{33}^o)^2 \\ + 4 \cos^2 \theta \sin^2 \theta p_{44} \epsilon_{11}^o \epsilon_{33}^o & - 2 p_{44} \epsilon_{11}^o \epsilon_{33}^o \cos 2\theta] \\ \cos \theta \sin \theta [-\sin^2 \theta p_{11}(\epsilon_{11}^o)^2 + \sin^2 \theta p_{31}(\epsilon_{33}^o)^2 & (\cos \theta \sin \theta)^2 [-(\epsilon_{11}^o)^2 (p_{13} - p_{11}) \\ - \cos^2 \theta p_{13}(\epsilon_{11}^o)^2 + \cos^2 \theta p_{33}(\epsilon_{33}^o)^2 & + (\epsilon_{33}^o)^2 (p_{33} - p_{31}) \\ - 2 p_{44} \epsilon_{11}^o \epsilon_{33}^o \cos 2\theta] & + p_{44} \epsilon_{11}^o \epsilon_{33}^o \cos^2 2\theta] \\ 0 & 0 \\ 0 & 0 \end{pmatrix}. \quad (55)$$

The fact that the fifth and the sixth lines of the condensed tensor (55) are equal to zero reveals that the following components of the dielectric tensor are zero as well:

$$\delta \epsilon_{12} = \delta \epsilon_{21} \equiv \delta \epsilon_6 = 0, \quad \delta \epsilon_{13} = \delta \epsilon_{31} \equiv \delta \epsilon_5 = 0. \quad (56)$$

Physically, Eq. (56) means that there is no coupling between the polarizations  $\vec{E}_1$  and  $\vec{E}_2$  which can be regarded as eigenmodes of polarization.

Each of the perturbed dielectric parameters  $\delta \epsilon_i$  are then deduced from

$$\delta \epsilon_i = - (N_{IJ})_{L_i, C_j} S_j, \quad (57)$$

where  $L_i$  is the  $i$ th row of the  $(N_{IJ})_{C_3, C_4}$  matrix (55) (since  $S_j$  is either  $S_3$  or  $S_4$ ).

### C. Solution by first-order perturbation theory

The last set of equations (48)–(50) can be then simplified, thanks to Eqs. (56) and (50), and by introducing the indices of refraction  $n_o$  and  $n_e$ ,

$$\frac{\partial^2 E_{1,1}}{\partial x_3^2} + \frac{\omega^2}{c^2} n_o^2 E_{1,1} = \delta_1 E_{1,0}, \quad (58)$$

$$\frac{\partial^2 E_{2,1}}{\partial x_3^2} + \frac{\omega^2}{c^2} n_e^2 E_{2,1} = \delta_2 E_{2,0}, \quad (59)$$

$$\epsilon_{23} E_{2,1} + \epsilon_{33} E_{3,1} = -\delta \epsilon_{3i} E_{i,0}, \quad (60)$$

where

$$\delta_1 = -\frac{\omega^2}{c^2} \delta \epsilon_{11} \quad (61a)$$

$$\equiv \frac{\omega^2}{c^2} (N_{IJ})_{1,3m}, \quad (61b)$$

$$\delta_2 = -\frac{\omega^2}{c^2} [\delta \epsilon_{22} - 2(\epsilon_{23}/\epsilon_{33}) \delta \epsilon_{23} + (\epsilon_{23}/\epsilon_{33})^2 \delta \epsilon_{33}] \quad (62a)$$

$$\equiv \frac{\omega^2}{c^2} (N_{IJ})_{2,3m}. \quad (62b)$$

In anticipation of Sec. IV E, we introduce the  $(N_{IJ})_{k,3m}$  coefficients, derived from Eq. (57), where the  $k$  index refers to the probe polarization direction [either  $x_1$  ( $k=1$ ) or  $x_2$  ( $k=2$ )] and the  $3m$  index (either 33 or 32) denotes the acoustic polarization of the  $S_j$  strain,

$$(N_{IJ})_{1,3m} \equiv (N_{IJ})_{L_1, C_j}, \quad (63)$$

$$(N_{IJ})_{2,3m} \equiv (N_{IJ})_{L_2, C_j} - 2(\epsilon_{23}/\epsilon_{33})(N_{IJ})_{L_4, C_j} \\ + (\epsilon_{23}/\epsilon_{33})^2 (N_{IJ})_{L_3, C_j}. \quad (64)$$

Solution of Eqs. (58) and (59) is the key to the first-order perturbation solution leading to the general expression of the electric field. A particular solution of the first-order perturbed electric field is inspired from plane waves,

$$E_{k,1} = E_{k,1}^*(x_3) e^{i\omega[t - (n_k/c)x_3]}, \quad (65)$$

where  $n_k$  corresponds to  $n_o$  for  $k=1$  and to  $n_e$  for  $k=2$ , and  $E_{k,1}^*(x_3)$  is the spatially inhomogeneous amplitude of the scattered field. By inserting the formal solutions Eq. (65) into the differential equations (58) and (59), we obtain a new differential equation,

$$\frac{\partial^2 E_{k,1}^*}{\partial x_3^2} - 2j\omega(n_k/c) \frac{\partial E_{k,1}^*}{\partial x_3} = \delta_k(x_3) E_{k,0}^o, \quad (66)$$

with  $k=1,2$ . By assuming that the particular electric field solution and its first derivative is zero at infinity, an integration from infinity to  $x_3$  gives

$$\frac{\partial E_{k,1}^*}{\partial x_3} - 2j\omega(n_k/c) E_{k,1}^* = \int_{+\infty}^{x_3} E_{k,0}^o \delta_k(x'_3) dx'_3. \quad (67)$$

The particular solution of Eq. (67) can then be assumed in the form

$$E_{k,1}^* = A(x_3) e^{2j\omega(n_k/c)x_3}, \quad (68)$$

where  $A(x_3)$  is the spatially inhomogeneous amplitude of the scattered field. By inserting (68) into Eq. (67), we obtain

$$\frac{\partial A}{\partial x_3} = \left( \int_{+\infty}^{x_3} E_{k,0}^o \delta_k(x'_3) dx'_3 \right) e^{-2j\omega(n_k/c)x_3}. \quad (69)$$

Integration of Eq. (69) gives

$$A = E_{k,0}^o \int_{+\infty}^{x_3} \left( \int_{+\infty}^{x'_3} \delta_k(x''_3) dx''_3 \right) e^{-2j\omega(n_k/c)x'_3} dx'_3. \quad (70)$$

The double integral can be rewritten in the form

$$A = E_{k,0}^o \int_{+\infty}^{x_3} \delta_k(x''_3) \left( \int_{x''_3}^{x'_3} e^{-2j\omega(n_k/c)x'_3} dx'_3 \right) dx''_3 \quad (71)$$

to yield

$$A = E_{k,0}^o \int_{+\infty}^{x_3} \delta_k(x''_3) \frac{e^{-2j\omega(n_k/c)x_3} - e^{-2j\omega(n_k/c)x''_3}}{-2j\omega(n_k/c)} dx''_3. \quad (72)$$

The particular solution of Eq. (68) becomes

$$E_{k,1}^* = E_{k,0}^o \int_{+\infty}^{x_3} \delta_k(x''_3) \frac{1 - e^{-2j\omega(n_k/c)(x''_3 - x_3)}}{-2j\omega(n_k/c)} dx''_3. \quad (73)$$

The final formal expression of the particular solution of the first order is deduced from Eqs. (65) and (73),

$$\begin{aligned} E_{k,1} = & \left( \int_{+\infty}^0 \frac{\delta_k(x''_3)}{-2j\omega(n_k/c)} dx''_3 \right. \\ & - \int_0^{x_3} \frac{\delta_k(x''_3)}{2j\omega(n_k/c)} dx''_3 \left. \right) E_{k,0}^o e^{j\omega[t - (n_k/c)x_3]} \\ & + \left( \int_{+\infty}^{x_3} \delta_k(x''_3) \frac{e^{-2j\omega(n_k/c)x''_3}}{2j\omega(n_k/c)} dx''_3 \right) E_{k,0}^o e^{j\omega[t + (n_k/c)x_3]}. \end{aligned} \quad (74)$$

The homogeneous solutions that propagate in both directions, namely,  $C_1 e^{j\omega[t - (n_k/c)x_3]}$  and  $C_2 e^{j\omega[t + (n_k/c)x_3]}$ , are then added to Eq. (74) in order to obtain the final solution of the scattered electric field. We obtain

$$\begin{aligned} E_{k,1} = & \left( \int_{+\infty}^0 \frac{\delta_k(x''_3)}{-2j\omega(n_k/c)} dx''_3 \right. \\ & - \int_0^{x_3} \frac{\delta_k(x''_3)}{2j\omega(n_k/c)} dx''_3 + C_1 \left. \right) E_{k,0}^o e^{j\omega[t - (n_k/c)x_3]} \\ & + \left( \int_{+\infty}^{x_3} \delta_k(x''_3) \frac{e^{-2j\omega(n_k/c)x''_3}}{2j\omega(n_k/c)} dx''_3 + C_2 \right) E_{k,0}^o e^{j\omega[t + (n_k/c)x_3]}. \end{aligned} \quad (75)$$

The constant  $C_1$  is found from the condition that at the surface  $x_3=0$ , the amplitude of the electromagnetic wave propagating towards  $+x_3$  should be equal to the amplitude of the launched electromagnetic wave. Moreover, due to radiation boundary conditions at  $x_3=+\infty$ , the  $C_2$  constant must be zero. Finally, the general solution of the scattered electric field is

$$\begin{aligned} E_k = & E_{k,0}^o e^{j\omega[t - (n_k/c)x_3]} \left( 1 - \int_0^{x_3} \frac{\delta_k(x''_3)}{2j\omega(n_k/c)} dx''_3 \right) \\ & + E_{k,0}^o e^{j\omega[t + (n_k/c)x_3]} \int_{+\infty}^{x_3} \frac{\delta_k(x''_3)}{2j\omega(n_k/c)} e^{-2j\omega(n_k/c)x''_3} dx''_3. \end{aligned} \quad (76)$$

The first term in Eq. (76) describes the loss of the incident electric field that is partially backscattered to the front surface. The second term of Eq. (76) corresponds to the Brillouin scattering of the electric field.

#### D. Reflectivity coefficients

Assessing the optical reflection coefficients for the sample configuration of Fig. 4, air/transparent film/opaque crystal requires the use of the Maxwell equations at the boundaries. The sequence of the analytical treatment begins with the determination of the reflection coefficients at the transparent-film/opaque-crystal boundary followed by the treatment of the whole air/transparent-film/opaque-crystal assembly. Following this, the value of Eq. (76) when  $x_3=0$  gives the electric field at the boundary of the crystal surface,

$$E_k(0) = E_{k,0}^o e^{j\omega t} (1 + D_k), \quad (77)$$

where

$$D_k = \int_{+\infty}^0 \frac{\delta_k(x''_3)}{2j\omega(n_k/c)} e^{-2j\omega(n_k/c)x''_3} dx''_3. \quad (78)$$

The magnetic field at the boundary is given by Faraday's law, which can be expressed as

$$-\frac{\partial E_2}{\partial x_3} - j\omega B_1 = 0, \quad (79)$$

$$\frac{\partial E_1}{\partial x_3} - j\omega B_2 = 0 \quad (80)$$

$$-j\omega B_3 = 0. \quad (81)$$

Spatial differentiation of Eq. (76) gives

$$\frac{\partial E_k}{\partial x_3}(0) = -j\omega(n_k/c)E_{k,0}^o(1 - D_k), \quad (82)$$

and the magnetic-field components at the boundary satisfy

$$B_1(0) = (n_2/c)E_{2,0}^o e^{j\omega t}(1 - D_2), \quad (83)$$

$$B_2(0) = - (n_1/c)E_{1,0}^o e^{j\omega t}(1 - D_1), \quad (84)$$

$$B_3(0) = 0. \quad (85)$$

The optical reflection coefficients at the transparent-film/opaque-crystal interface will be defined by

$$E_{F,k}^-(0) = r_{kk}E_{F,k}^+(0), \quad (86)$$

where  $k=1,2$ . The superscript + indicates an incident electric field propagating in the  $x'_3 > 0$  direction whereas - indicates a reflected field propagating in the  $x'_3 < 0$  direction. The index  $F$  indicates the film medium. Since there is no coupling between the electric fields  $E_1 \leftrightarrow E_2$ , the off-diagonal reflection coefficients  $r_{12}$  and  $r_{21}$  cancel. The continuity of the electric field at the transparent-film/opaque-crystal boundary, coming from Faraday's law, gives

$$E_{F,k}^+(0)(1 + r_{kk}) = E_k(0) = E_{k,0}^o(1 + D_k). \quad (87)$$

Since surface density charges are incorporated inside the complex dielectric constants, Faraday's law enforces the continuity of the tangential components of the magnetic field and we obtain

$$(n_k/c)E_{F,k}^+(1 - r_{kk}) = B_k(0). \quad (88)$$

Taking into account Eqs. (78), (83), and (84), we obtain

$$(n_k/c)E_{F,k}^+(1 - r_{kk}) = (n_k/c)E_{k,0}^o(1 - D_k). \quad (89)$$

The combination of the set of equations (87) and (89) allows the determination of the reflection coefficients  $r_{kk}$ ,

$$r_{kk} = \frac{D_k(n_F + n_k) + n_F - n_k}{D_k(n_F - n_k) + n_F + n_k}, \quad (90)$$

where  $k=1,2$ , and  $n_F$  is the isotropic index of refraction of the transparent medium. The fact that the  $D_k$  coefficients, that incorporate the acoustic perturbation, are assumed to be small ( $D_k \ll 1$ ) allows us to perform a first-order Taylor expansion of Eq. (90),

$$r_{kk} \sim \frac{n_F - n_k}{n_F + n_k} + D_k \frac{4n_F n_k}{(n_F + n_k)^2} \quad (91a)$$

$$\equiv r_{kk,0} + r_{kk,1}, \quad (91b)$$

where  $r_{kk,0}$  is the zero-order reflection coefficient and  $r_{kk,1}$  the first-order reflection coefficient that involves the acoustic perturbation.

The two reflection coefficients  $r_{kk}^o = E_{air,k}^-/E_{air,k}^+$  of the whole air/transparent-film/opaque-crystal assembly appear in the continuity of the electric- and magnetic-field components at the air/isotropic-film boundary, respectively, written in the form

$$E_{air,k}^+(e^{jk_{air}H} + r_{kk}^o e^{-jk_{air}H}) = E_{F,k}^+(e^{jk_F H} + r_{kk} e^{-jk_F H}), \quad (92)$$

$$E_{air,k}^+(-e^{jk_{air}H} + r_{kk}^o e^{-jk_{air}H}) = -n_F E_{F,k}^+(e^{jk_F H} - r_{kk} e^{-jk_F H}), \quad (93)$$

where  $k_{air} = \omega/c$ ,  $k_F = n_F \omega/c$ , and  $H$  is the transparent-film thickness. The electric fields in air and inside are assumed to be of the form  $E_{air,k}^\pm e^{j(\omega t \mp k_{air} x_3)}$  and  $E_{F,k}^\pm e^{j(\omega t \mp k_F x_3)}$ . A straightforward division of Eq. (92) by Eq. (93) gives

$$\frac{e^{-2jk_{air}H} + r_{kk}^o}{e^{-2jk_{air}H} - r_{kk}^o} = \frac{1 + r_{kk} e^{-2jk_F H}}{n_F(1 - r_{kk} e^{-2jk_F H})}, \quad (94)$$

and we obtain

$$r_{kk}^o = \frac{r_{kk} e^{-2jk_F H}(1 + n_F) + 1 - n_F}{r_{kk} e^{-2jk_F H}(1 - n_F) + 1 + n_F} e^{2jk_{air}H}. \quad (95)$$

The phase term  $e^{-2jk_F H}$  expresses the interferometric process that occurs with the superposition of the electric fields reflected from the two air/transparent-film and transparent-film/opaque-crystal interfaces.

The reflectivity technique that has been experimentally carried out is sensitive to the differential modification of the light reflectivity coefficient that satisfies

$$\Delta R_k = d(|r_{kk,0}^o|^2), \quad (96)$$

where  $r_{kk,0}^o$  is the reflection coefficient without acoustic perturbation, transposed from Eq. (95) by changing  $r_{kk}$  into  $r_{kk,0}$  of Eq. (91b). The following analytical treatment consists in calculating the modulus of Eq. (95) and its derivative. The modulus of Eq. (95) satisfies

$$|r_{kk,0}^o|^2 = \frac{|r_{kk,0}|^2(1 + n_F)^2 + (1 - n_F)^2 + 2(1 - n_F^2)\text{Re}(r_{kk,0} e^{-2jk_i H})}{|r_{kk,0}|^2(1 - n_F)^2 + (1 + n_F)^2 + 2(1 - n_F^2)\text{Re}(r_{kk,0} e^{-2jk_i H})}. \quad (97)$$

Afterward, the differentiation of Eq. (97) yields

$$\begin{aligned} \Delta R_k = & \frac{32n_F\{(1 + n_F^2) + (1 - n_F^2)\text{Re}(r_{kk,0} e^{-2jk_i H})\}\text{Re}(r_{kk,0} r_{kk,1}^*)}{[|r_{kk,0}|^2(1 - n_F)^2 + (1 + n_F)^2 + 2(1 - n_F^2)\text{Re}(r_{kk,0} e^{-2jk_i H})]^2} + \frac{8n_F(1 - n_F^2)(1 - |r_{kk,0}^o|^2)\text{Re}(r_{kk,1} e^{-2jk_i H})}{[|r_{kk,0}|^2(1 - n_F)^2 + (1 + n_F)^2 + 2(1 - n_F^2)\text{Re}(r_{kk,0} e^{-2jk_i H})]^2} \\ & + \frac{8n_F(1 - n_F^2)(1 - |r_{kk,0}^o|^2)\text{Im}(r_{kk,0} e^{-2jk_i H})d(2k_i H)}{[|r_{kk,0}|^2(1 - n_F)^2 + (1 + n_F)^2 + 2(1 - n_F^2)\text{Re}(r_{kk,0} e^{-2jk_i H})]^2}. \end{aligned} \quad (98)$$

We recall that the differential reflectivity  $\Delta R_k$  is expressed here for an arbitrary electric-field polarization  $k$ . For the general case, the differential reflectivity would be a linear combination of the contributions of both cross-polarized scattered electric field  $\vec{E}_1$  (i.e.,  $k=1$ ) and  $\vec{E}_2$  (i.e.,  $k=2$ ) such as  $\Delta R = \Delta R_1 + \Delta R_2$ . The term  $r_{kk,1}(x_3, t)$  characterizes the contribution of the photoelastic coupling [see Eqs. (78) and (90)], which appears in the first two terms of Eq. (98). The last term of Eq. (98) characterizes the contribution of interferometric sensitivity; a slight modification of the film thickness  $H$ , caused by an acoustical displacement of  $x_3$  polarization, induces a modification of the optical path that in turn modifies the optical interference. Actually, the whole Eq. (98) underscores that by choosing the film thickness  $H$ , the detection of photoelastic perturbations could be enhanced at the same time as the interferometric contribution is canceled [when the term  $\text{Im}(r_{kk,0}e^{-2jk_iH})$  is canceled, the photoelastic term  $\text{Re}(r_{kk,0}e^{-2jk_iH})$  of Eq. (98) is enhanced]. In the following, we will neglect the interferometric sensitivity contribution that has been removed on purpose by a proper choice of the film thickness  $H$ .

### E. Analytical synthesis of the reflectivity variation

The aim of this section is to link the theory of thermoelastic generation to the theory of photoelastic detection. In other words, we will describe a means of getting the general analytical reflectivity variation  $\Delta R$  that takes into account the formulation of the thermoelastically induced acoustic strains.

As soon as the parameters  $r_{kk,1}$  that involve the photoelastic coupling through the  $D_k$  coefficients are expressed, the difference in reflectivity  $\Delta R$  that gives the trace of the strain acoustic wave can be numerically evaluated (the optical parameters  $n_i$ ,  $n_k$  are known, hence  $r_{kk,0}$  is easily evaluated as well). In fact, the task consists in getting the general  $D_k$  terms that follow the strain acoustic field. Because each of the incident strains that penetrate the crystal, either longitudinal  $S'_{33}$  or shear  $S'_{32}$ , is decomposed into two strain components of the QL and QS modes, it is necessary to evaluate the amplitudes of these corresponding modes. Each of these strains matches the incident strain waves that satisfies, in the coordinate axes of the crystal,

$$S'_{3i}(x_3, t) = - \left( \frac{\alpha F}{\rho c_p} \right) \frac{v_m}{v_i} \beta_{im} e^{-\alpha v_m(t-x_3/v_i)}. \quad (99)$$

We recall that the existence (absence) of the prime index denotes the isotropic film (anisotropic substrate). The negative sign comes from the total acoustic reflection at the film/air interface. The  $(-1)^{i+1}$  coefficients disappear from Eq. (37) because  $x'_3$  has been replaced by  $x_3$ . The QL and QS strains launched in the crystal are proportional to the following strains  $S'_{3i}$ , transposed from Eq. (99) when  $v'_i$  is replaced by  $v_q$ :

$$S^q_{3i}(x_3, t) = - \left( \frac{\alpha F}{\rho c_p} \right) \frac{v_m}{v_i} \beta_{im} e^{-\alpha v_m(t-x_3/v_q)}, \quad (100)$$

where  $q$  denotes the QL mode for  $q=3$  and the QS mode for  $q=2$ . Moreover, the amount of the QL and QS strains effec-

tively transmitted through the interface is weighted by the acoustic transmission coefficients that carefully distinguish each of the components  $S^q_{33}$  and  $S^q_{32}$  contributions to the strain. Moreover, the evaluation of the strain  $S^q_{3i}$  at the  $3m$  coordinate, obtained from the  $3i$  incident strain component and for the  $q$  quasimode, written in the form

$$S^q_{3m,3i} = T^q_{3m,q} S^q_{3i}, \quad (101)$$

involves the coefficients  $T^q_{3m,q}$  that are the acoustic transmission coefficients of the  $3m$  strain components; the superscript  $3i$  of  $S^q_{3m,q}$  denotes the acoustic polarization of the incident wave (i.e., from the film F) and the  $q$  coefficient the polarization of the induced quasimode. The technique of calculation of the acoustic transmission coefficients  $T^q_{3m,q}$  of the  $3m$  strain component, inspired by the academic theory of acoustic transmission at the interface of two solids, is described in Ref. 37. We obtain

$$\begin{aligned} T^{33}_{33,3} &= - \left( \frac{v'_3}{v_3} \right) \sin \alpha \frac{2z'_3(z'_2 + z_2) \cos \alpha}{d}, \\ T^{33}_{33,2} &= \left( \frac{v'_3}{v_2} \right) \cos \alpha \frac{-2z'_3(z'_2 + z_3) \sin \alpha}{d}, \\ T^{33}_{32,3} &= \left( \frac{v'_3}{v_3} \right) \cos \alpha \frac{2z'_3(z'_2 + z_2) \cos \alpha}{d}, \\ T^{33}_{32,2} &= \left( \frac{v'_3}{v_2} \right) \sin \alpha \frac{-2z'_3(z'_2 + z_3) \sin \alpha}{d}, \\ T^{32}_{33,3} &= - \left( \frac{v'_2}{v_3} \right) \sin \alpha \frac{-2z'_3(z'_2 + z_3) \sin \alpha}{d}, \\ T^{32}_{33,2} &= \left( \frac{v'_2}{v_2} \right) \cos \alpha \frac{-2z'_3(z'_2 + z_3) \sin \alpha}{d}, \\ T^{32}_{32,3} &= \left( \frac{v'_2}{v_3} \right) \cos \alpha \frac{-2z'_3(z'_2 + z_3) \sin \alpha}{d}, \\ T^{32}_{32,2} &= \left( \frac{v'_2}{v_2} \right) \sin \alpha \frac{-2z'_3(z'_2 + z_3) \sin \alpha}{d}, \end{aligned} \quad (102)$$

where the denominator  $d$  is

$$d = (z'_3 + z_3)(z'_2 + z_2) + \sin^2 \alpha (z'_3 + z'_2)(z_2 - z_3),$$

$z'_3$ ,  $z'_2$ ,  $z_3$ , and  $z_2$  are the acoustic impedances of the L, S, QL, and QS modes, respectively, and  $\alpha$  is the angle between the QL polarization and the  $x_3$  axis. Given the induced strain  $S^q_{3m,q}$ , we deduce the following  $D_k$  term, according to Eq. (78):

$$D_k^{3i} = \frac{\omega^2}{c^2} \frac{(N_{IJ})_{k,3m}}{2j\omega(n_k/c)} \int_{+\infty}^0 S^q_{3m,q} e^{-2j\omega(n_k/c)x_3} dx_3, \quad (103)$$

where the superscript  $3i$  has been introduced to denote the polarization of the incident strain  $S^q_{3i}$ . The coefficients

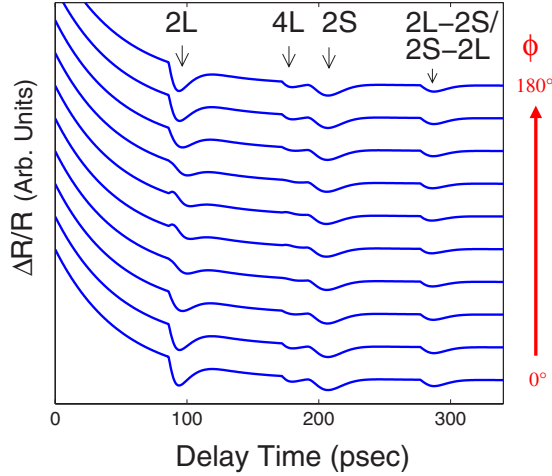


FIG. 8. (Color online) Full numerical simulations of the reflectivity measurements shown in Fig. 4. The photoelastic coefficients that match our experimental observations are  $p_{12}=41p_{13}$ ,  $p_{31}=8p_{13}$ ,  $p_{11}=-5p_{13}$ ,  $p_{33}=-97p_{13}$ , and  $p_{44}=-9p_{13}$ , where  $p_{13}$  is a negative imaginary number. The thermal contribution was taken into account by an exponential background.

$(N_{IJ})_{k,3m}$  can be estimated from Eqs. (63) and (64). This expression for  $D_k$  is given for a probe polarized along  $x_1$  ( $k=1$ ) or along  $x_2$  ( $k=2$ ); for intermediate directions, the general reflected light  $\Delta R$  will be due to a linear superposition of the two orthogonally polarized polarization of the probes, namely,  $\Delta R(D_1^{3i})$  and  $\Delta R(D_2^{3i})$ .

This last expression (103) finalizes the task of linking both theories.

## V. DISCUSSION

Thanks to the picture of both the thermoelastic generation process and the reflectivity detection process provided by the theoretical analyses of Secs. III and IV, we are able to perform full numerical simulations of the transient reflectivity measurements. The unknowns are the photoelastic coefficients  $p_{ij}$  of the Zn hexagonal crystal. With a single set of the following six photoelastic coefficients,  $p_{11}=-5p_{13}$ ,  $p_{33}=-97p_{13}$ ,  $p_{44}=-9p_{13}$ ,  $p_{12}=41p_{13}$ ,  $p_{31}=8p_{13}$ , where  $p_{13}$  is a negative imaginary number (as in the case of an ideal metal), a mean-square procedure results in a satisfactory simulation of the transient reflectivity signals as a function of the probe polarization or as a function of the Zn crystal tilt angle  $\theta$ . Figure 8 shows a simulation of the transient reflectivity of the signal presented in Fig. 4, for a fixed angle  $\theta$  of  $36^\circ$  and for several angles  $\phi$  of probe polarization (when  $\phi=0^\circ$ , the polarization is in the  $+x_2$  direction of the crystal, and when  $\phi=180^\circ$ , the probe polarization is in the  $-x_2$  direction). The numerical values of the acoustic reflective coefficients, detailed in Ref. 37, are  $R_{LL}\sim-0.2$ ,  $R_{SS}\sim-0.08$ ,  $R_{LS}\sim-0.45$ , and  $R_{SL}\sim-0.03$ . From the numerical values of  $R_{LS}$  and  $R_{SL}$ , the 2L-2S/2S-2L echo appears to be almost 94% of shear polarization nature.

Concretely, it can be mentioned that such a tilt configuration expands the possibilities of picosecond acoustics by pro-

viding a different means of measuring the photoelastic coefficients of the metallic substrate under consideration, in conjunction with the theory detailed in the present paper. In fact, the full set of Zn photoelastic coefficients (normalized to  $p_{13}$  in our case) is deduced from a single experiment, whereas just one photoelastic coefficient is accessible from a typical picosecond acoustic sample configuration.

Our numerical calculations attest that the theory can provide a complete picture of the recorded signals, in particular, concerning the shape of the recorded 2L and 2S echoes that appear to be extremely sensitive to the direction of the probe's polarization. For a qualitative interpretation of the drastic polarization dependence (see Figs. 4 and 8), the change in reflectivity  $\Delta R$  can be presented in the following contracted form, following Eq. (103):

$$\Delta R_k^{3i} \sim \int_0^\infty f_{3m,k}(x_3) S_{3m,q}^{3i} dx_3. \quad (104)$$

Here,  $f_{3m,k}(x_3)$  is the normalized sensitivity distribution function as a function of the direction of probe's polarization, given by the  $k$  index ( $k=1$ , ordinary;  $k=2$ , extraordinary), and on the acoustic polarization of the strain  $S_{3m,q}^{3i}$ , given by the  $3m$  index. The  $q$  index, which indicates the nature of the quasimode, results in an implicit summation of the strain  $S_{3m,q}^{3i}$  that can be expanded in the following way:

$$S_{3m,q}^{3i} = T_{3m,2}^{3i} S_{3i}^2 + T_{3m,3}^{3i} S_{3i}^3 \equiv T_{3m,2}^{3i} S'_{3i}(t - x_3/v_2) + T_{3m,3}^{3i} S'_{3i}(t - x_3/v_3), \quad (105)$$

where

$$S'_{3i}(\xi) = - \left( \frac{\alpha F}{\rho c_p} \right) \frac{v_m}{v_i} \beta_{im} e^{-\alpha v_m(\xi)} \quad (106)$$

is the mathematical strain function of the  $\xi$  variable that comes from Eq. (99). Approximating the sensitivity function  $f_{3m,k}(x_3)$  beneath the surface of the metallic substrate as a Dirac delta, Eq. (105) leads to

$$\Delta R_k^{3i} \approx S'_{3i}(0,t) [T_{3m,2}^{3i} + T_{3m,3}^{3i}] \int_0^\infty f_{3m,k}(x_3) dx_3 - \frac{\partial S'_{3i}}{\partial t}(0,t) \times \left[ \frac{T_{3m,2}^{3i}}{v_2} + \frac{T_{3m,3}^{3i}}{v_3} \right] \int_0^\infty x_3 f_{3m,k}(x_3) dx_3. \quad (107)$$

This truncated Taylor expansion is based on a smallness of the light penetration length  $l_e$  relative to the length  $l_a$  of the detected acoustic strain. The contribution  $\sim \partial S'_{3i}/\partial t$  can be estimated to be  $l_a/l_e \gg 1$  times smaller than of  $\sim S'_{3i}(t)$ . However, owing to the asynchrony of the acoustic eigenmodes ( $v_3 \neq v_2$ ), the two coefficients in the square brackets in Eq. (107) are different, and it can happen that, for a particular polarization of the probe that significantly reduces the magnitude of the first term, the second term is not necessarily reduced, and the signal proportional to the strain rate  $\partial S'_{3i}(t)/\partial t$  can dominate. This is exactly the qualitative reason for the differentiation of the signal profile in a transition from extraordinary to ordinary light probe for the 2L echoes

reported in Fig. 4 and numerically reproduced in Fig. 8. In fact, the sensitivity to the strain rate acoustic field, that has been observed for an ordinary probe polarization (i.e.,  $x_1$  direction), is another mark of the asynchrony of propagation of the quasimodes QL and QS.

A remarkable feature of the dependence on probe polarization direction is the coincidence of the signals for  $\phi=0^\circ$  and  $\phi=180^\circ$ , that is equivalent either to rotation of the crystal by  $180^\circ$  or to transformation of the tilted angle from  $\theta$  to  $-\theta$ . This coincidence highlights that the reflectivity measurement is actually symmetric with respect to a  $\pi$  rotation of the crystal or an inversion of the tilted angle  $\theta$ . To theoretically investigate this property, we return to the analysis of the scattering phenomena of the electric field by the acoustic strain field, that is governed by the following coefficients [see Eqs. (61a) and (62a)]:

$$\delta_1 = -\frac{\omega^2}{c^2} \delta\epsilon_{11}, \quad (108)$$

$$\delta_2 = -\frac{\omega^2}{c^2} [\delta\epsilon_{22} - 2(\epsilon_{23}/\epsilon_{33})\delta\epsilon_{23} + (\epsilon_{23}/\epsilon_{33})^2\delta\epsilon_{33}]. \quad (109)$$

Using the expression of the perturbed dielectric tensor given in Eq. (57), it is easy to show that a transformation of  $\theta$  into  $-\theta$  introduces a change of sign into the pertinent components of the extended photoelastic tensor ( $N_{IJ}$ ) as follows:

$$\begin{aligned} (N_{IJ})_{L_1,C_3}(\theta) &= (N_{IJ})_{L_1,C_3}(-\theta), \\ (N_{IJ})_{L_1,C_4}(\theta) &= -(N_{IJ})_{L_1,C_4}(-\theta), \\ (N_{IJ})_{L_2,C_3}(\theta) &= (N_{IJ})_{L_2,C_3}(-\theta), \\ (N_{IJ})_{L_2,C_4}(\theta) &= -(N_{IJ})_{L_2,C_4}(-\theta), \\ (N_{IJ})_{L_3,C_3}(\theta) &= (N_{IJ})_{L_3,C_3}(-\theta), \\ (N_{IJ})_{L_3,C_4}(\theta) &= -(N_{IJ})_{L_3,C_4}(-\theta), \\ (N_{IJ})_{L_4,C_3}(\theta) &= -(N_{IJ})_{L_4,C_3}(-\theta), \\ (N_{IJ})_{L_4,C_4}(\theta) &= -(N_{IJ})_{L_4,C_4}(-\theta). \end{aligned} \quad (110)$$

For clarity, the components of the photoelastic tensor ( $N_{IJ}$ ) are labeled according to the index of the line  $L_I$  and to that of the column  $C_J$ . Taking into account that the transformation of  $\theta$  into  $-\theta$  affects the sign of the shear  $S_{23} \equiv S_4$  and longitudinal  $S_{33} \equiv S_3$  strains according to

$$\begin{aligned} S_4(\theta) &= -S_4(-\theta), \\ S_3(\theta) &= S_3(-\theta), \end{aligned} \quad (111)$$

the transformations of the perturbed dielectric tensor are predicted to be

$$\begin{aligned} \delta\epsilon_{11}(\theta) &= \delta\epsilon_{11}(-\theta), \\ \delta\epsilon_{22}(\theta) &= \delta\epsilon_{22}(-\theta), \end{aligned} \quad (112)$$

$$\begin{aligned} \delta\epsilon_{33}(\theta) &= \delta\epsilon_{33}(-\theta), \\ \delta\epsilon_{23}(\theta) &= -\delta\epsilon_{23}(-\theta). \end{aligned} \quad (113)$$

Since

$$\frac{\epsilon_{23}(\theta)}{\epsilon_{33}(\theta)} = -\frac{\epsilon_{23}(-\theta)}{\epsilon_{33}(-\theta)}, \quad (114)$$

we obtain the following important results:

$$\delta_1(-\theta) = -\frac{\omega^2}{c^2} \delta\epsilon_{11}(\theta) = \delta_1(\theta), \quad (115)$$

$$\begin{aligned} \delta_2(-\theta) &= -\frac{\omega^2}{c^2} \{ \delta\epsilon_{22}(\theta) - 2[\epsilon_{23}(\theta)/\epsilon_{33}(\theta)]\delta\epsilon_{23}(\theta) \\ &\quad + [\epsilon_{23}(\theta)/\epsilon_{33}(\theta)]^2\delta\epsilon_{33}(\theta) \} = \delta_2(\theta). \end{aligned} \quad (116)$$

As a consequence, the probe light is scattered in the same way when the crystal disorientation is changed from  $\theta$  to  $-\theta$ , which is equivalent to a  $\pi$  rotation of the crystal. In other words, the reflectivity measurement is not sensitive to the sign of the tilt angle  $\theta$  (i.e.,  $\theta$  or  $-\theta$  is the same).

Important practical application of this finding is the possibility of generating and detecting picosecond shear strain pulses by the use of polycrystalline samples, whose crystallites are naturally randomly oriented. Thus, even if the average shear strain over the whole assembly of the crystallites involved is almost zero due to the random orientation and/or disorientation of the grains (mathematically speaking  $\langle S_4(\theta) \rangle \sim 0$ ), it is not so for the average shear strain reflectivity signal which integrates all the individual reflectivity signals of the crystallites without cancellation (mathematically speaking  $\langle \Delta R(\theta) \rangle \neq 0$ ). There is no cancellation of the total shear strain scattered electric field if the generation and the detection of the acoustic waves both take place locally in the same crystallite. These theoretical arguments explain the possibility of using polycrystalline materials for the generation and detection of shear picosecond strains, and have been successfully experimentally confirmed (see Fig. 9). The use of a Zn polycrystalline substrate, mechanically polished and layered by a ZnO transparent layer, demonstrates an almost equivalent efficiency of generation and detection of shear strain pulses as for Zn single crystals. By comparison of the size of the laser spots (diameter  $\sim 40 \mu\text{m}$ ) with the size of the grains, it appears that each recorded picosecond transient reflectivity signal averages over tens of grains (see Fig. 10). Since the picosecond acoustic contribution of the  $\theta \sim 0^\circ$  grains is much smaller (see the inset of Fig. 3) compared to other favorable grain orientations that permit shear wave generation, the shear acoustic pulses are systematically detected. In addition, the modification of the shape of the recorded longitudinal pulses of Fig. 9 is understood within the framework of the probe's polarization dependence described above; this tells about the average angle of orientation  $\langle \phi(\theta) \rangle$

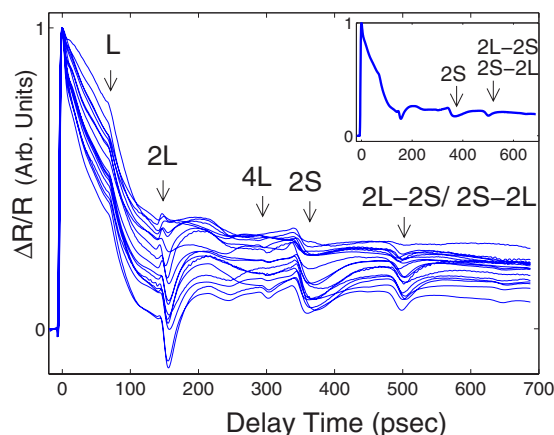


FIG. 9. (Color online) Changes in transient reflectivity observed in the case of a polycrystalline Zn substrate coated by a ZnO film of 350 nm thickness, at different points of the surface, separated by tens of laser spot size dimensions. The inset shows the spatially averaged signal.

of the local crystallites, as long as the acoustic diffraction length is larger than the acoustic wave propagation length.

## VI. CONCLUSION

In summary, we have reported essential features of the generation and detection of plane hypersound pulses in single-crystal and polycrystalline samples. The detection of these pulses takes place in the crystals and proved to be sensitive to the probe linear polarization orientation. These results are promising not only for the realistic routine use of picosecond shear pulses to the noncontact evaluation of thin films but also in the field of ultrafast tribology. Indeed, the ability to excite and detect shear picosecond collimated acoustic beams and multibeams is not only of fundamental interest but is also a considerable step toward the practical implementation of purely optical methods in ultrafast spectroscopy of solids, liquids, and interfaces. The liquid film for

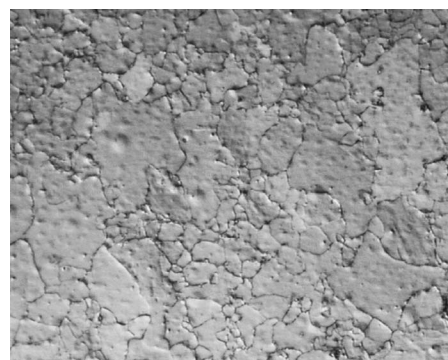


FIG. 10. Microscope polarimetric image of the Zn polycrystalline sample. The real image is  $64 \times 48 \mu\text{m}^2$ . The crystallite sizes vary from 1 to 10  $\mu\text{m}$ .

testing could be deposited directly on the metallic generator and/or detector of shear hypersound or on a dielectric transparent film covering it; this dielectric film may serve as an acoustic delay line as well as an acoustic impedance matching medium.<sup>38</sup> For example, one of the challenging problems would be the study of ultrafast relaxation mechanisms of ions in liquids, which are still debated. The brief characteristic times of short-range reorganization in liquids or melted crystals are indeed investigated through inelastic x-ray scattering.<sup>39</sup> Therefore, probing viscoelastic properties of liquids with very high frequency shear waves could obviously provide different insights on the ultrafast relaxation processes. Moreover, laser ultrasonics is well adapted for probing surface, interface, or confined volumes where liquids can also exhibit a departure from bulklike behavior, as shown recently.<sup>40</sup>

## ACKNOWLEDGMENTS

The authors acknowledge the technical support by P. Laffez, C. Launay, M. Zaghrioui, and B. Duclos (from Struers company). The authors thank D. Torchinsky for fruitful scientific discussions.

\*Also at Keith Nelson Group, Massachusetts Institute of Technology, Cambridge, MA USA. Electronic address: pezeril@mit.edu

<sup>1</sup>G. A. Askar'yan, A. M. Prokhorov, G. F. Chanturiya, and G. P. Shipulo, *Sov. Phys. JETP* **17**, 1463 (1963).

<sup>2</sup>R. M. White, *J. Appl. Phys.* **34**, 3559 (1963).

<sup>3</sup>C. Thomsen, J. Strait, Z. Vardeny, H. J. Maris, J. Tauc, and J. J. Hauser, *Phys. Rev. Lett.* **53**, 989 (1984).

<sup>4</sup>C. Thomsen, H. T. Grahn, H. J. Maris, and J. Tauc, *Phys. Rev. B* **34**, 4129 (1986).

<sup>5</sup>P. Hess, *Phys. Today* **55**(3), 42 (2002).

<sup>6</sup>J. A. Rogers, A. Maznev, M. J. Banet, and K. A. Nelson, *Annu. Rev. Mater. Sci.* **30**, 117 (2000).

<sup>7</sup>K. A. Nelson, *J. Appl. Phys.* **53**, 6060 (1982).

<sup>8</sup>V. Gusev and A. Karabutov, *Laser Optoacoustics* (AIP, New York, 1993).

<sup>9</sup>C. Rossignol, J. M. Rampnoux, M. Pertion, B. Audoin, and S.

Dilhaire, *Phys. Rev. Lett.* **94**, 166106 (2005).

<sup>10</sup>S. I. Zolotov, V. V. Krylov, E. P. Ponomarev, and T. V. Shtentsel, *Sov. Phys. Acoust.* **31**, 344 (1985).

<sup>11</sup>L. M. Lyamshev and B. I. Chelnokov, *Sov. Phys. Acoust.* **29**, 220 (1983).

<sup>12</sup>A. Harata, H. Nishimura, and T. Sawada, *Appl. Phys. Lett.* **57**, 132 (1990).

<sup>13</sup>M. D. Fayer, *IEEE J. Quantum Electron.* **QE-22**, 1437 (1986).

<sup>14</sup>A. A. Karabutov, M. P. Matrosov, and N. B. Podymova, *Acoust. Phys.* **39**, 196 (1993).

<sup>15</sup>V. Gusev, P. Picart, D. Mounier, and J.-M. Breteau, *Opt. Commun.* **204**, 229 (2002).

<sup>16</sup>W. Grill and O. Weiss, *Phys. Rev. Lett.* **35**, 588 (1975).

<sup>17</sup>W. E. Bron, M. Rossinelli, Y. H. Bai, and F. Keilmann, *Phys. Rev. B* **27**, 1370 (1983).

<sup>18</sup>D. H. Hurley, O. B. Wright, O. Matsuda, V. E. Gusev, and O. V.

- Kolosov, *Ultrasonics* **38**, 470 (2000).
- <sup>19</sup>T. Bienville and B. Perrin, in Proceedings of the WCU, 2003 (unpublished), p. 813, [sfa.asso.fr/wcu2003/procs/website/](http://sfa.asso.fr/wcu2003/procs/website/)
- <sup>20</sup>O. Matsuda, O. B. Wright, D. H. Hurley, V. E. Gusev, and K. Shimizu, *Phys. Rev. Lett.* **93**, 095501 (2004).
- <sup>21</sup>T. Pezeril, N. Chigarev, P. Ruello, S. Gougeon, D. Mounier, J.-M. Breteau, P. Picart, and V. Gusev, *Phys. Rev. B* **73**, 132301 (2006).
- <sup>22</sup>J. A. Hildebrand, *J. Acoust. Soc. Am.* **79**, 1457 (1986).
- <sup>23</sup>M. Dubois, F. Enguehard, L. Bertrand, M. Choquet, and J. P. Monchalain, *Appl. Phys. Lett.* **64**, 554 (1994).
- <sup>24</sup>D. H. Hurley, *J. Acoust. Soc. Am.* **115**, 2054 (2004).
- <sup>25</sup>T. Pezeril, V. Gusev, D. Mounier, N. Chigarev, and P. Ruello, *J. Phys. D* **38**, 1421 (2005).
- <sup>26</sup>*Handbook of Optics* (sponsored by the Optical Society of America, McGraw-Hill, New York, 1995).
- <sup>27</sup>*CRC Handbook of Chemistry and Physics*, 82nd ed., edited by D. R. Lide (CRC, Boca Raton, FL, 2001).
- <sup>28</sup>O. B. Wright and V. E. Gusev, *IEEE Trans. Ultrason. Ferroelectr. Freq. Control* **42**, 331 (1995).
- <sup>29</sup>R. Daudliker and J.-F. Willemin, *Opt. Lett.* **6**, 165 (1981).
- <sup>30</sup>A. D. W. McKie and J. W. Wagner, *Appl. Phys. Lett.* **53**, 1043 (1988).
- <sup>31</sup>V. Gusev, *Acust. Acta Acust.* **82**, 37 (1996).
- <sup>32</sup>O. Matsuda and O. B. Wright, *Anal. Sci.* **17**, s216 (2001).
- <sup>33</sup>O. Matsuda and O. B. Wright, *J. Opt. Soc. Am. B* **19**, 3028 (2002).
- <sup>34</sup>O. Matsuda and O. B. Wright, *Rev. Sci. Instrum.* **74**, 895 (2003).
- <sup>35</sup>D. F. Nelson and M. Lax, *Phys. Rev. Lett.* **24**, 379 (1970).
- <sup>36</sup>J. F. Nye, *Physical Properties of Crystals* (Oxford University Press, Oxford, 1957).
- <sup>37</sup>T. Pezeril, Ph.D. thesis, Université du Maine, <http://tel.ccsd.cnrs.fr/tel-00011291>
- <sup>38</sup>G. Tas and H. J. Maris, *Phys. Rev. B* **55**, 1852 (1997).
- <sup>39</sup>G. Ruocco, F. Sette, M. Krisch, U. Bergmann, C. Masciovecchio, and R. Verbeni, *Phys. Rev. B* **54**, 14892 (1996).
- <sup>40</sup>H. Reichert, F. Bencivenga, B. Wehinger, M. Krisch, F. Sette, and H. Dosch, *Phys. Rev. Lett.* **98**, 096104 (2007).